

**This is a non-peer-reviewed preprint submitted to EarthArXiv.**

**This manuscript has been submitted to Elementa: Science of the Anthropocene**

**Canada's Landfill Methane Inventories: The Challenge of Accurate Modeled and Measurement-Based Emissions**

**Jordan Stuart (1), Evelise Bournon (1), Rebecca Martino (1), Lindelwa Coyle (1), Susan Fraser (2), Emil Laurin (2), Felix Vogel (2), Nicholas Bishop (2), Sebastien Ars (2), David Risk (1,\*)**

**(1) FluxLab, Department of Earth and Environmental Sciences, St. Francis Xavier University, Nova Scotia, Canada**

**(2) Environment and Climate Change Canada, Ontario, Canada**

**\*Corresponding author: David Risk ([drisk@stfx.ca](mailto:drisk@stfx.ca))**

1 Canada's Landfill Methane Inventories: The Challenge of Accurate Modeled and  
2 Measurement-Based Emissions

3 Jordan Stuart<sup>1</sup>, Evelise Bourlon<sup>1</sup>, Rebecca Martino<sup>1</sup>, Lindelwa Coyle<sup>1</sup>, Susan Fraser<sup>2</sup>, Emil Laurin<sup>2</sup>, Felix  
4 Vogel<sup>2</sup>, Nicholas Bishop<sup>2</sup>, Sebastien Ars<sup>2</sup>, David Risk<sup>1,\*</sup>

5 <sup>1</sup>FluxLab, Department of Earth and Environmental Sciences, St. Francis Xavier University, Nova Scotia,  
6 Canada

7 <sup>2</sup>Environment and Climate Change Canada, Ontario, Canada

8 \*Corresponding author: David Risk [drisk@stfx.ca](mailto:drisk@stfx.ca)

9

## 10 Abstract

11 We present a measurement-based assessment of methane emissions from 42 landfills across diverse  
12 climatic regions in Canada. Our findings reveal that emission rates predicted by the First Order Decay  
13 (FOD) model used by Environment and Climate Change Canada at the visited sites are substantially  
14 higher than most measured emission rates, on average by a factor of 3, particularly for cold and arid  
15 climates typical of the Canadian prairie provinces (by a factor of 13 on average). Bias-corrected  
16 measurement rates aligned more closely with values reported to the Canadian Greenhouse Gas Reporting  
17 Program. Compared to the amounts estimated by the FOD model, our measurement-based estimations  
18 show greater variation with changes in climate. At some warmer and wetter sites, measured rates  
19 exceeded FOD modeled estimates, underscoring the influence of climate on landfill methane dynamics  
20 and FOD model behavior. We also found that measurement-based estimates yield more realistic methane  
21 collection effectiveness values than those implied by Canada's FOD-based inventories. Canadian  
22 regulations are based on mitigation strategies that are built on the outcomes of such FOD models. Our  
23 results suggest that the current FOD inventory model parameters—that include decay rates and oxidation  
24 assumptions—should be refined to better reflect site-specific conditions and climate variability across  
25 Canada.

26

## 27 Introduction

28 Like many countries, Canada's waste sector is a major source of methane emissions, emitting an  
29 estimated 19 Mt CO<sub>2</sub>e in 2023, or 0.51 t CO<sub>2</sub>e per capita (Environment and Climate Change Canada,  
30 2025). To track greenhouse gas emissions in the waste sector, Environment and Climate Change Canada  
31 (ECCC) compiles Canada's landfill methane inventory using a variation of the Intergovernmental Panel  
32 on Climate Change (IPCC) First Order Decay (FOD) waste model with default parameters or national,  
33 provincial, or site-level parameters when available (Pipatti and Svardal, 2006). Though this model is used  
34 by ECCC to estimate emissions at the provincial level for greenhouse gas reporting in its National  
35 Inventory Report of Greenhouse Gas Sources and Sinks in Canada (NIR), it can be configured to estimate  
36 site-specific emissions by incorporating available operational information, waste tonnage, waste  
37 composition, waste age, decay rate, and methane generation potential. Calculation of methane emission is  
38 based on modeled methane generation adjusted for any methane destruction (accounting for flaring  
39 efficiency) or utilization and methane oxidation of the generated methane that is not recovered in landfill  
40 covers (the IPCC default oxidation factor of 0.1 is used for all regions and years; ECCC, 2025). At  
41 municipal solid waste landfills, ECCC (2025; section 7.2.3) estimated the emission uncertainty to be  
42 ±76% using the default parameters from the IPCC 2006 Guidelines (IPCC, 2006). Gaps in input activity  
43 timeseries are completed with interpolated or extrapolated values (ECCC, 2025).

44 In addition to compiling Canada's methane inventory, ECCC administers Canada's Greenhouse Gas  
45 Reporting Program (GHGRP). Landfills emitting 10 kt CO<sub>2</sub>e/year or more are required to report  
46 emissions to the GHGRP. However, unlike in the United States, where GHGRP data are integrated into  
47 its national inventory estimates (EPA, 2023), Canada uses them to compare and validate its inventory.  
48 Canadian landfills reporting to the GHGRP are not required to use a standard methodology. Some  
49 operators rely on engineering calculations using the IPCC FOD model or alternatives such as the United  
50 States Environmental Protection Agency's LandGEM model.

51 Differences in methodology contribute to observed discrepancies between operator-reported GHGRP  
52 values and the ECCC's IPCC-based estimates. Based on our subset of landfills, the ECCC-modeled  
53 emissions are typically higher on a site-by-site basis—sometimes only marginally, but in some cases,  
54 more than nine times higher. Such inconsistencies are increasingly problematic because national  
55 inventories face government and public scrutiny. Discrepancies between modeled and measured landfill  
56 methane emissions are well-documented, with international studies reporting underestimations of up to  
57 200% in individual and governmental inventories (Wang et al., 2024; Scarpelli et al., 2024; Cusworth et  
58 al., 2024). In the United States, two recent studies found that measured emissions exceeded American  
59 GHGRP-reported values in 47% of cases and were, on average, 2.7 times higher across all American  
60 landfills (Scarpelli et al., 2024; Cusworth et al., 2024). In Canada, Thompson et al. (2009) found that the  
61 Scholl Canyon model often overestimated methane recovery rates, and LandGEM consistently  
62 underestimated them.

63 The inaccuracy of waste models is due to several factors. Many landfill methane models rely on  
64 environmental parameters that are challenging to validate. For example, the moisture content can vary  
65 significantly in both space and time due to the heterogeneous nature of landfill waste, which in turn  
66 affects the estimation of leachate generation and the amount of anaerobic decomposition. Sampling waste  
67 to estimate its moisture often requires heavy equipment and still may not yield representative results  
68 (Krause et al., 2023). Also, models often fail to account for seasonal and climatic variability (Gollapalli  
69 and Kota, 2018). For example, Scheutz et al. (2011) reported lower-than-expected methane emissions in  
70 Denmark due to precipitation patterns, temporal variability, and landfill characteristics. Similarly, Jain et  
71 al. (2021) observed lower emissions from landfills in arid regions compared to wetter climates. Among  
72 our selected sites, six of the ten most significant differences between ECCC modeled emissions and  
73 GHGRP reports are from Alberta and Saskatchewan, regions where annual precipitation may be as low as  
74 250 mm. Effectively mitigating methane depends on accurate inventories so that interventions can be  
75 identified and prioritized. In its National Inventory Report (ECCC, 2025), ECCC acknowledges landfill

76 methane emissions as the largest source of uncertainty at the national level. Landfill methane regulations  
77 have been released to reduce waste-sector methane, but the ability to accurately measure the impact of  
78 regulations will depend on how well landfill methane emissions and their sources can be quantified.  
79 Reducing inventory uncertainty will require improving the quality of the FOD model input data from  
80 Canada’s approximately 270 large landfills, which account for more than 85% of Canada’s methane  
81 landfill emissions (ECCC, 2022). Furthermore, improving data collection will enhance model validation  
82 capabilities.

83 Measuring methane emissions comes with several challenges that often stem from temporal changes in  
84 weather conditions—particularly fluctuations in barometric pressure and wind speed (Fredenslund et al.,  
85 2010; Kissas et al., 2022)—limited site accessibility, complex dispersion patterns caused by wind  
86 conditions, topography or obstacles, and the heterogeneous nature of landfill methane sources (Lando et  
87 al., 2017; Fjelsted et al., 2019). In rapid screening survey campaigns like the one presented in this study,  
88 measurement attempts are not always successful.

89 This study compares measurement-based landfill methane emission rates with those modeled by ECCC  
90 using the IPCC FOD model and those reported to GHGRP. We also examine how climate variability  
91 affects measured emissions and their divergence from FOD-modelled emissions, considering factors such  
92 as the accumulated waste size, the waste methane potential, and the effectiveness of methane collection  
93 systems.

## 94 Methods

### 95 *Site Locations*

96 From July to November 2022, we surveyed landfills across Canada, with or without methane collection  
97 systems, varying in size and operational status (open or closed). Surveys were conducted sequentially  
98 using two mobile laboratories: one that began in Nova Scotia on Canada’s Atlantic coast and moved

99 westward to Ontario, and another that began in Saskatchewan and continued westward toward British  
100 Columbia on Canada's Pacific coast. Most of our measurements were taken on public roads where no  
101 permit was required, and safe driving remained the priority. A list of 150 locations was established before  
102 the campaign, but weather, instrument issues or inadequate timing prevented us from surveying them all.  
103 Unpredictable local weather changes were a factor in reducing the number of landfills visited. We strive  
104 to avoid taking measurements immediately after or during weather changes, primarily for fieldwork safety  
105 and because rapid changes in barometric pressure have been linked to landfill emission events (barometric  
106 pumping; Fredenslund et al, 2010; Xu et al., 2014; Kissas et al., 2022). Taking measurements during a  
107 barometric pressure decrease would have led to higher emission estimates, so we favored a more  
108 conservative approach. However, we acknowledge that our emission snapshots are biased downward  
109 relative to annual emission estimates. For our analysis, we focused on 42 sites (Figure 1), out of 111  
110 surveyed landfills, where we had obtained off-site emission rate estimates under the following conditions:  
111 wind speeds within an appropriate range, no weather change, an unobstructed line of sight to the landfill,  
112 and no issues with measurement instrumentation.

### 113 *Measurements*

114 For the landfill emission measurement campaign, we used two mobile survey laboratories. Each mobile  
115 laboratory consisted of a Toyota RAV4 outfitted with a Picarro gas analyzer (G2210-i CRDS, Picarro  
116 Inc., USA) connected to a high-volume 7 LPM pre-pump. The setup minimized the lag time between the  
117 external air inlet and the instrument. At the front of the vehicle, we mounted the air inlet on a mast fixed  
118 to the vehicle's roof. An open Y-splitter fitting allowed excess airflow to be released. The mast also  
119 housed a 2-axis ultrasonic anemometer (WindSonic, Gill Instruments Ltd, UK), an electric compass  
120 (Model 32500, RM Young, USA), and a GPS (18x, Garmin Ltd, USA). All mast-mounted equipment was  
121 approximately 2.5 m above ground level. A data logger (CR1000X, Campbell Scientific, USA) recorded  
122 all measurements, including internal time, at 2 Hz.

123 Both gas analyzers were calibrated before the campaign using two gas standards with different CH<sub>4</sub>  
124 mixing ratios, prepared by the AmeriFlux Management Program (Lawrence Berkeley National  
125 Laboratory, Berkeley, CA, USA) and referenced to within <1 ppb of the World Meteorological  
126 Organization CH<sub>4</sub> scale using standards maintained by the U.S. National Oceanic and Atmospheric  
127 Administration. We used AmeriFlux standard FB03987 (4.52 ppm CH<sub>4</sub>, 516.54 ppm CO<sub>2</sub>, prepared  
128 August 2019), for which we found an average departure of 0.008 ppm CH<sub>4</sub>, and AmeriFlux standard  
129 FB04007 (1.81 ppm CH<sub>4</sub>, 385.18 ppm CO<sub>2</sub>, prepared August 2019), for which the average offset was  
130  $5.6 \times 10^{-4}$  ppm CH<sub>4</sub>. Before measuring the standards, the analyzer cavity was purged for several hours  
131 with zero–water-vapor gas until H<sub>2</sub>O levels stabilized below 0.05%. Both gas analyzers were checked  
132 immediately after the campaign using the same procedure to assess drift over the course of the campaign.

133 During fieldwork, we conducted a second daily check: each morning, we benchmarked each Picarro  
134 analyzer with a target gas containing known CO<sub>2</sub> and CH<sub>4</sub> mixing ratios. The cylinder was attached for  
135 five minutes to monitor any deviation between the known and measured values. While field benchmarks  
136 are inherently more variable than laboratory tests, our field benchmarks were sufficient for detecting  
137 major drift, which we did not observe.

138 Each morning, we also measured the lag time between the inlet and analyzer cavity by introducing CH<sub>4</sub>  
139 pulses at the inlet and timing how long it took the pulses to arrive at the analyzer. The measured lag time  
140 ensured that the gas mixing ratio measurements with the GPS locations were precisely aligned. To  
141 confirm that the slower response time of the Picarro G2210-i adequately captured plumes, we compared  
142 our measurements with the measurements of two faster analyzers, a Licor LI7810 and a Picarro G2401,  
143 used in a simultaneous companion survey conducted by ECCO. While our Picarro model damped peak  
144 CH<sub>4</sub> values and extended plume duration, the areas under the curve were equal between the analyzers  
145 (Figures S1 and S2).

146 We conducted downwind transect measurements across one or multiple plumes, progressing from  
147 background levels to peak values and back. We repeated each transect up to 15 times at speeds ranging  
148 from 15 to 80 km/h, depending on safety and traffic conditions. When operators granted us landfill  
149 access, we also conducted on-site measurements to better characterize potential emission sources.  
150 However, in this study, we only used the off-site downwind measurements to estimate emission rates.

### 151 *Data Processing and Selecting Transects*

152 Following the data quality checks, we calculated true wind vectors using measured wind speeds, compass  
153 readings, and GPS data. We calculated the Sun's position and collected meteorological data from the  
154 nearest airport that included cloudiness, ceiling height, and wind to estimate atmospheric stability classes  
155 using Turner's method (Turner, 1964). We excluded transects collected when wind speeds were less than  
156 1.5 m/s, during highly unstable conditions (Pasquill stability class "A"), or during the night (Pasquill  
157 stability classes "E" and "F").

158 We estimated the ambient methane level using iterative mean suppression (Liland, 2015), and we defined  
159 methane enhancements to be the difference between measured and ambient levels. We discarded the  
160 transects that had no significant methane enhancement ( $<0.01$  ppm), relative to the instrument precision,  
161 noise level, and estimated background variation.

162 We mapped and assessed the remaining transect locations relative to landfill boundaries. Using Google  
163 imagery and Street View, we identified potential obstacles to dispersion (e.g., tall buildings or dense  
164 forests) and screened for nearby non-landfill methane sources such as dairy and poultry farms, compost  
165 facilities, water treatment plants, cattle exchange centers, and oil and gas infrastructure. We excluded the  
166 transects influenced by such obstacles or additional methane sources. Finally, we calculated the distance  
167 between each landfill and its associated methane enhancements, retaining only transects where this  
168 distance was less than 2.5 km. This 2.5 km distance was selected based on the results of a controlled-  
169 release experiment (our approach is identified as Truck A in Hossain et al., 2025), in which emission rates

170 were largely underestimated at this distance. Because our slow-response gas instrument produced  
171 methane enhancements with amplitudes and widths similar to the background methane level, they were  
172 barely discernible and were often underestimated during the controlled release experiment.

### 173 *Estimating Emission Rates*

174 To estimate the landfill emission rates from the measured methane enhancements, we used a Gaussian  
175 dispersion model. Gaussian dispersion models are widely used to simulate air pollutant dispersion and  
176 have effectively estimated biogas emissions from landfills (Fredenslund et al., 2019; Aronica et al., 2009).  
177 While Gaussian methods are somewhat less accurate than tracer gas approaches, they are faster to  
178 implement, do not require site access, and cost roughly two-thirds less, making them well-suited for  
179 screening studies like ours (Fredenslund et al., 2019; Fallah-Shorshani et al., 2017; Matacchiera et al.,  
180 2019).

181 Many Canadian landfills are in remote areas with limited road networks, often forcing transects to be near  
182 landfill fence lines where multiple Gaussian peaks have been observed because several methane sources  
183 within a landfill operation are present (Cusworth et al., 2024). In contrast to Fredenslund et al. (2019), we  
184 found that it was not always possible to model a completely coalesced plume or to assume the landfill  
185 center was the main source of methane. In our case, we did not know the source locations and emission  
186 rates. Our approach was like that of Gillespie et al. (2025) and Ars et al. (2020), which involved  
187 minimizing differences between the observed enhancements and Gaussian model predictions. Unlike  
188 Gillespie's approach, which used either the known centers of emitting features of the landfill or the  
189 corners of the landfill as potential emitting sources, we used random sets of potential emitting points  
190 sampled from gridded locations within landfill boundaries, and then we simultaneously calculated their  
191 emission rates. Both Gillespie's approach and ours were tested concurrently at a controlled methane  
192 release site, producing similar rate estimates (Hossain, 2025). The Gaussian model accounted for  
193 parameters including source–measurement distances, source and measurement heights above ground,

194 wind speed, and dispersion coefficients (sigma parameters). We assumed that the corrected wind at the  
195 measurement location reflected the wind at the source, and that the source emissions were continuous. We  
196 derived the dispersion parameters from the Pasquill-Gifford-Turner model for open-country settings,  
197 based on atmospheric stability. Our algorithm estimates the total landfill emission rate by adjusting the  
198 contribution from each source to ensure that the sum of modeled methane concentrations matches the  
199 measured methane enhancements. More information on the Gaussian Plume Model and the inversion is  
200 available in the Supporting Information. We retained only those results for which the total modeled  
201 methane enhancement fell between 80% and 200% of the measured enhancement along downwind  
202 transects. We calculated the total landfill emission rates by summing the individual source rates. We  
203 repeated this operation over 1000 random distributions of sources, and each landfill was attributed the  
204 average and standard deviation of the estimated rate ensemble.

205 Atmospheric conditions, such as wind and stability class, can influence the uncertainties in emission rate  
206 estimates. Landfills, due to their topography and heat generation, often create localized microclimates,  
207 which means that meteorological parameters measured on nearby roads or at airports might not perfectly  
208 represent conditions at the emission sources. We analyzed emissions assuming fixed source heights (4 m  
209 above road level) and variable heights from high-resolution digital elevation models (HRDEM; Natural  
210 Resources Canada) but found no significant differences in estimated rates. Source height was not a critical  
211 parameter when measurements were taken hundreds of meters from the sources.

212 To evaluate uncertainty and bias, we conducted a controlled release experiment at a closed landfill with a  
213 gas collection system (Hossain et al., 2025). This included 35 double-blind tests downwind of eight point  
214 sources and two area sources (>200 m<sup>2</sup>) spread over 10 ha, emitting 25 kg/h to 250 kg/h. Our method,  
215 identified as “Truck A” in the study, consistently captured 66% of true emissions (including both the  
216 controlled release and the landfill emissions), with an uncertainty of  $\pm 47.6\%$  across rates from 0 kg/h to  
217 238 kg/h (Hossain et al., 2025). When measurements were collected nearly 2.5 km away or with forested  
218 obstacles between the landfill and the mobile laboratory, the resulting emission rates of the controlled

219 release experiment tended to be underestimated. To minimize underestimating the emissions rates in this  
220 study, we avoided having distant transects and obstructed lines of sight.

221 We present the emission rate estimates directly from the Gaussian inversion and as bias-corrected values  
222 (adjusted by  $1/0.66$ ). Fredenslund et al. (2019) observed a similar downward bias, reporting a factor of  
223 0.72 when they validated a Gaussian model using tracer-gas-correlation results in a study involving 91  
224 landfills across Denmark.

### 225 *Landfill categories*

226 We categorized landfills by area and climate. For landfill size binning, we divided the 42 landfills into  
227 three equal groups—small, medium, and large—based on each site's accumulated waste in place as  
228 calculated by ECCC (Figure 2). Our sites span over 5,000 km from Canada's Atlantic coast to its Pacific  
229 coast, encompassing climates that range from high-altitude, steppe-like conditions to mild, wet  
230 environments. The length of the growing season and the duration of the winter vary greatly from place to  
231 place. For climate classification, we initially used Köppen climate zones, but found most landfills  
232 clustered within a single zone, in particular, the humid continental zone. To select some of the FOD  
233 model parameters, ECCC uses the aridity index, the ratio of precipitation over the potential  
234 evapotranspiration (PET), to define two climate zones across Canada: one PET exceeds precipitation  
235 (aridity  $< 1$ ; "dry" climate) and another where PET is lower than precipitation (aridity  $> 1$ ; "wet"  
236 climate). At our selected sites, the aridity and the precipitation are roughly linearly related (Figure S5);  
237 the PET do not vary much. To refine the classification, we extracted weather data from local ECCC  
238 stations within 50 km of each landfill, including measured daily or hourly precipitation (rain and snow)  
239 and measured temperature records from 2018 to 2022. From these data, we calculated annual total  
240 precipitation and mean air temperature, averaged over the five past years preceding our measurement  
241 campaign. A temperature versus precipitation diagram enabled us to visually cluster the site into five  
242 climate categories (see the cluster extents on Figure 2):

- 243 • lower precipitation and lower temperature,
- 244 • lower precipitation and mid temperature,
- 245 • mid precipitation and higher temperature,
- 246 • higher precipitation and mid temperature, and
- 247 • much higher precipitation and/or much higher temperature.

248 These categories are relative to our dataset of 42 landfills, for which we defined “much higher”  
249 temperature as having an annual mean temperature above 10°C and “much higher” precipitation as over  
250 1750 mm/year; they are only based on the visual inspection of Figure 2, and not based on Canada’s or the  
251 world’s climate zones. More details about the climate clustering are provided in Section S2 of the  
252 Supplementary Material. When mapped (Figure 1), the categories revealed meaningful geographic  
253 patterns, with wetter climates concentrated along the west and east coasts and colder climates at higher  
254 northern latitudes.

### 255 *Comparing Measurement Estimates with FOD Modeled Values*

256 Unlike the ECCC and GHGRP annual emission estimates, our measurement-based rates represent  
257 instantaneous (“snapshot”) landfill emissions, primarily during summer (38 sites visited during summer; 6  
258 during fall). Canada’s extreme seasonality means summer temperatures can exceed winter values by more  
259 than 30°C. The seasonal variability calls into question some of the parameterization of the FOD model.  
260 At all sites, ECCC includes a 10% methane oxidation factor on the portion of methane that is not  
261 collected to account for methanotrophs in landfill biocovers reducing fugitive methane emissions. This is  
262 the default IPCC oxidation value, based on studies by Czepiel et al. (1996a, b) at a New Hampshire  
263 landfill. It represents an annual average, with actual oxidation likely negligible in winter but potentially  
264 high in summer. Optimal oxidation rates are reported at 25°C to 35°C (Spokas and Bogner, 2011), but  
265 methanotrophs can utilize CH<sub>4</sub> at far lower temperatures with an optimal temperature of 3.5°C to 10°C  
266 (Omelchenko et al., 1993), and methanotrophic activity has been observed at 1-2°C (Scheutz and

267 Kjeldsen, 2004; Einola et al., 2007). Chanton et al. (2009, 2011) found annual oxidation fractions ranging  
268 from 11% to 89%, with a mean of 35%. Also, Canadian landfills are often capped with thick layers of  
269 clay and soil rather than geotextile covers; this operational choice potentially increases oxidation when  
270 conditions are favorable. To assess the potential impact of a higher oxidation factor on FOD-modeled  
271 emission rates under warm, microbially active summer conditions, we compared measurement-based  
272 estimates with the standard ECCC modeled rates (10% oxidation) and with an adjusted model assuming a  
273 higher oxidation factor of 35%. This is only for comparison purposes (Figure 5), and we are not  
274 suggesting that the oxidation rate is 35% during the summer in Canada. We calculated the adjusted ECCC  
275 modeled emission rates by dividing original model estimates by  $\sim 1.4 [(1-0.1)/(1-0.35)]$ .

## 276 Results

### 277 *On-site Observations*

278 We gained access to 50% of the sites, which allowed us to better characterize methane sources and  
279 identify landfill areas with the highest emissions. Across these sites, the largest emissions were  
280 consistently observed at the active working faces, where new waste was deposited daily. These areas  
281 typically lacked covers and had not been integrated into landfill gas collection systems, making them  
282 major contributors to fugitive methane. Beyond the active working faces, we recorded elevated methane  
283 levels around manholes and leachate wells. In some cases, we also detected methane peaks downwind of  
284 compost piles during humid weather; however, compost-related methane enhancements were low or  
285 absent. Furthermore, we found that operational activities influenced emission patterns. We measured the  
286 highest on-site methane mixing ratios during construction activities, such as the installation of landfill gas  
287 collection systems, manholes, and leachate wells. These locations frequently produced methane levels  
288 high enough to saturate our analyzer (30 ppm). Occasionally, we were on site when leachate wells were  
289 being emptied, and at these times, we observed significant methane spikes.

290 *Comparing our Measurement-based Values to ECCC Modeled Values and GHGRP Industry-*  
291 *Reported Values*

292 We obtained ECCC modeled annual methane emission rates for 2022 at 40 of the 42 sites and emission  
293 rates for 2021 for 2 landfills. It should be noted that the 2021 modeled rates are based on a slightly  
294 different input parameter estimation approach, although they are derived from the same IPCC FOD  
295 model. The ECCC 2022 dataset also included annual measured methane flaring and collection amounts  
296 from a voluntary survey of landfill operators conducted by ECCC, and estimations of methane generation  
297 potential ( $L_0$  in tons of  $CH_4$ ), especially the accumulated  $L_0$  that accounts for  $L_0$  remaining in the landfill  
298 after previous decay. The  $L_0$  represents the potential amount of methane that could be generated from the  
299 landfill waste. Of 42 landfills, 31 reported flared and/or utilized methane amounts in 2022. It is unclear  
300 whether the sites for which we lack this information do not have a collection system or simply did not  
301 report it. We collected industry-reported emission rates for 2022 from the Canadian GHGRP database for  
302 33 of the 42 sites. The measured, modeled, and reported emission estimates are presented in Figure 3. The  
303 ECCC rates were consistently the highest of the two types of rates, ranging from near 0 kg/h to 2368 kg/h  
304 (mean: 471 kg/h), whereas the GHGRP rates ranged from 36 kg/h to 1511 kg/h (mean: 357 kg/h). With an  
305 oxidation rate of 35%, the ECCC rates range from near 0 kg/h to 1710 kg/h, with a mean of 340 kg/h,  
306 closer to the GHGRP range. Our direct measurement-based rates were generally lower than the ECCC or  
307 GHGRP rates, ranging from 3 kg/h to 511 kg/h with a mean of 118 kg/h. When we applied the bias  
308 correction from the controlled release experiment, our adjusted rates ranged from 5 kg/h to 774 kg/h  
309 (mean: 179 kg/h).

310 The GHGRP and ECCC rate distributions had a primary mode at 178 kg/h, whereas the measurement-  
311 based rate distribution peaked at 30 kg/h (Figure 4). However, the bias-corrected measurement-based  
312 distribution and GHGRP distribution shared a secondary mode from around 690 kg/h to 750 kg/h.

313 The ECCC emission rates exceeded 39 direct measurement-based rates and 37 bias-corrected  
314 measurement-based rates out of 42 sites (resp. 93% and 88%) and were higher than the GHGRP-reported  
315 rates for 20 of 33 sites (61%). In contrast, direct measurement-based rates surpassed GHGRP-reported  
316 values for only 4 of 33 sites (12%), and bias-corrected rates exceeded GHGRP values for 9 of 33 sites  
317 (27%). The five sites where our bias-corrected estimated rates exceeded the ECCC modeled rates are all  
318 in wet climate categories. Of the five, two have similar rates, with a difference of less than 10kg/h. For  
319 the three other sites, the ECCC modeled rates are also lower than the GHGRP rates.

320 We found that the highest emission rates were from open landfills. Of the 42 sites we visited, 9.5% (4  
321 sites) were closed; that is, they no longer accepted waste and had completed final covers and landscaping.  
322 Some of these closed sites had been repurposed for recreational use (e.g., golf courses, dog parks). At  
323 closed sites, we observed relatively low bias-corrected emission rates (11 kg/h to 244 kg/h), which were  
324 close to ECCC FOD estimates (near 0 kg/h to 257 kg/h). However, for two of three closed sites, operators  
325 reported unusually high values to the GHGRP (449 kg/h and 779 kg/h), exceeding our measurement-  
326 based and the ECCC modeled estimates.

327 For subsequent analyses, we focused on the bias-corrected values because they compared more favorably  
328 to “true” emissions (i.e., the true release rates of the controlled release experiment by Hossain et al.  
329 (2025)) on the measurement days without altering patterns relative to the ECCC modeled or GHGRP  
330 values. On average, the ratio of the ECCC rates to the measurement-based rates was 3.3 for closed sites  
331 (mean difference: 57 kg/h) and 6.4 for open sites (mean difference: 317 kg/h). Overall, the bias-corrected  
332 measurement-based rates range compares better with the GHGRP range ( $R^2 = 0.636$ , slope = 0.529) than  
333 with the ECCC FOD range ( $R^2 = 0.627$ , slope = 0.335) (Figure 5). Adjusting the ECCC FOD estimates  
334 for 35% oxidation improved the comparison with our measurement-based rates ( $R^2 = 0.627$ , slope =  
335 0.463; Figure 5). However, when their respective uncertainties are accounted (76% for ECCC and 47.6%  
336 for measurement-based estimates), ECCC and measurement-based emission rate estimate ranges overlap,  
337 except for a few landfills located in the drier areas of our study.

338 It should be noted that our measurements assessed only the emitted methane, not the methane produced  
339 (the sum of the methane emitted, collected, and oxidized). Landfill operators report the amount of  
340 methane flared and/or utilized to ECCC, but we do not know the amount of microbially oxidized  
341 methane. Therefore, we calculated methane collection *effectiveness* (collected / emitted+collected) instead  
342 of collection efficiency (collected/produced). Lower measurement-based rates resulted in higher  
343 calculated collection effectiveness, with a median of 51% overall and 76% for the large landfills,  
344 consistent with engineering expectations for systems installed on covered landfill areas. In contrast, we  
345 found the collection effectiveness derived from the ECCC FOD estimates to be substantially lower, with a  
346 median of 20% overall and 52% for the large landfills (Figure 6). The greater efficiency observed at the  
347 largest sites (in terms of accumulated waste) may be attributed to their higher collection system coverage,  
348 as they have a larger ratio of closed cell area to active cell area compared to smaller sites. Figure 7 shows  
349 the distribution of effectiveness for two types of climates: “dry”, which combines the two lower  
350 precipitation categories, and “wet”, which comprises the mid, high, and higher precipitation climate  
351 categories. The measurement-based emission rates do not lead to any difference in effectiveness, with a  
352 similar range and the same median. However, the ECCC emission estimates suggest a large difference in  
353 effectiveness, with a lower effectiveness at “dry” sites than at “wet” sites.

354 As shown in Figure 8, relative to measurement-based rates, the ECCC underpredicts emissions in the  
355 warmest, wettest areas (the west coast). However, in drier climates, particularly in Canada’s arid central  
356 regions, the measurement-based rates diverged sharply from the ECCC FOD estimates, which are on  
357 average more than 12 times higher than the measured rates, likely because the model does not sufficiently  
358 account for the reduction of anaerobic waste degradation due to waste dryness.

## 359 Discussion

360 The key finding of this study is that measurement-based summer snapshots of methane emissions at  
361 Canadian landfills are on average lower than the annual emissions predicted by the ECCC FOD modeled

362 emissions. When expressed as percentages, the measurement-based emission rates are, on average, 77%,  
363 70%, 56% and 38% lower for the climate categories of lower precipitation and lower temperature, lower  
364 precipitation and mid temperature, mid precipitation and higher temperature and higher precipitation and  
365 mid temperature, respectively. The difference is -52% for the “much higher precipitation and/or much  
366 higher temperature” category. This divergence reflects a combination of factors: potential bias in the  
367 measurement technique, unrealistic model parameters, or both. Our rates were derived from field surveys  
368 conducted primarily during the summer with warm air temperatures and low wind speeds. Barometric  
369 pressure and temperature were measured at only a few landfills where sensor towers could be deployed,  
370 so these sparse records do not allow us to conclude anything about the influence of atmospheric pressure  
371 or temperature. In their 2025 study, Gillespie et al. examined how these drivers could affect  
372 measurement-based emission estimates at landfills in Ontario. They found that inclusion of these drivers  
373 improves the slope of the best-fit line compared to inventoried emissions, though it does not significantly  
374 alter the correlation coefficients. However, methane oxidation by landfill cover layers could be more  
375 effective during summer, when our surveys were conducted, than during winter, and could be higher than  
376 the 10% default annual oxidation factor assumed in the ECCC FOD modeling. Methanotroph activity  
377 depends on landfill cover characteristics and increases with temperature (Börjesson and Svensson, 1997;  
378 Park et al., 2005). Although cover properties vary among landfills and with environmental conditions,  
379 oxidation can be a significant factor in the differences between our measurement-based rates and ECCC  
380 FOD estimates, underscoring the importance of methanotrophs and covers in reducing landfill emissions.

381 This study also highlights the limitations of applying default or large-scale model parameters, especially  
382 decay rates ( $k$ ), across Canada’s diverse climate zones to model the methane generation at each landfill.  
383 Our measurement-based estimates were substantially variable depending on the climate zone. Figure 9  
384 illustrates methane generation (emitted + 10% oxidized + recovered) per accumulated methane generation  
385 potential  $L_0$  for each climate category. The  $\text{CH}_4$  generation potential  $L_0$  (in tonnes of  $\text{CH}_4$ ) is estimated  
386 from the mass of degradable organic matter multiplied by the fraction of landfill gas that is  $\text{CH}_4$  (1/2) and

387 the molecular weight ratio of CH<sub>4</sub> over C (16/12). Note that this L<sub>0</sub> definition is different from the one  
388 provided in the IPCC 2000 Good Practice Guidance, where it is expressed as tonnes of methane per  
389 tonnes of waste landfilled. The accumulated methane generation potential L<sub>0</sub> accounts for the previous  
390 year's L<sub>0</sub> decay. In the ECCC modeling, the amount of degradable organic matter is based on waste  
391 composition determined at the provincial level, not the site level, and does not account for any site-  
392 specific variability. As a result, ECCC might overestimate methane production at large urban landfills  
393 where organic waste diversion programs are active. Figure 9 illustrates the contrast between  
394 measurement-based methane generation per methane generation potential L<sub>0</sub>, which increases as the  
395 climate gets wetter and warmer, and the ECCC FOD-based methane generation, which displays bimodal  
396 variability—showing a similar amount at all the drier sites and a different, consistent amount at all the  
397 wetter sites. The measurement-based methane generation is lower than the model-based values except for  
398 the wettest climate zone. This could be an indication of a potential overestimation of the methane  
399 generation, hence the methane emission, especially in low precipitation areas. There is no clear  
400 relationship with the amount of landfill waste.

401 Assuming a methane generation time of 15 years followed by negligible generations, the measurement-  
402 based methane generation translates to a methane generation potential from the measurement-based rates  
403 of 1 m<sup>3</sup> to 56 m<sup>3</sup> CH<sub>4</sub> per tonne of total accumulated waste (the annual total amount of waste that remains  
404 after some water removal and decomposition), and 27 m<sup>3</sup> and 33 m<sup>3</sup> CH<sub>4</sub> per tonne of accumulated waste  
405 from ECCC FOD modeled methane generation for “dry” and “wet” climate respectively. In a review by  
406 Krause et al. (2016), methane generation potentials ranged from 20 m<sup>3</sup> to 223 m<sup>3</sup> CH<sub>4</sub> per tonne of  
407 municipal solid waste. Our values and ECCC values fall within the lower quarter of this range, which we  
408 expect for dry and cold Canadian conditions. However, ECCC values are higher than measurement-based  
409 values for all but the wettest and/or warmest sites.

410 The ECCC FOD estimates have a pronounced upward bias for cold and arid climates and underestimate  
411 emissions for the warmer and/or wetter areas (Figure 8). Vu et al. (2017) demonstrated that FOD models

412 with default parameters fail to capture methane production dynamics for cold semi-arid climates, with  
413 mean percentage errors ranging from 55% to 135%. We estimated the bulk landfill waste decay rates ( $k$ )  
414 both from our measurements, assuming a 10% methane oxidation, and the FOD-modeled rates, as:

$$k = -\ln \left( 1 - \frac{\textit{emitted+collected+oxidized}}{L_0} \right). \quad (1)$$

415 The values are reported in Table A. Decay rates vary widely by waste composition and moisture content,  
416 and nutrient availability, pH, and temperature are less significant factors. Our median  $k$  values vary from  
417 0.004 to 0.0063  $y^{-1}$ , from the coldest, driest sites to the warmest, wettest sites. The FOD-based  $k$  values,  
418 accounting for regional waste composition, are 0.03  $y^{-1}$  for the dry sites and 0.05  $y^{-1}$  for the wet sites. The  
419 values range within the range reported by Jain et al. (2021) from a study of 114 landfills in the United  
420 States, from 0.004 to 0.226  $y^{-1}$ , with a median of 0.068  $y^{-1}$ . Both Canadian FOD and measurement-based  $k$   
421 values fall within the lower half of the US  $k$  value range. This may be due to factors such as lower  
422 temperatures, prolonged sub-zero periods, reduced precipitation, and differences in waste composition  
423 resulting from distinct organic diversion practices. The measurement-based  $k$  values indicate that waste  
424 decay is significantly slower under dry and cold conditions than assumed by the FOD model. This  
425 disparity may be further amplified because our measurements were taken during the summer, which can  
426 be drier than other seasons and may affect waste moisture levels. The default IPCC bulk waste decay rate  
427 values—0.05  $y^{-1}$  for boreal/temperate dry climates and 0.09  $y^{-1}$  for boreal/temperate wet climates—are,  
428 on average, 1.7 times higher than the ECCC FOD values and over 3 times higher than the measurement-  
429 based estimates. More accurate decay rates and methane generation potentials tailored to Canadian  
430 climate zones could improve inventory estimates and scale them downward. Given Canada's rapidly  
431 changing climate, understanding methane generation under different environmental conditions is critical.  
432 Our findings emphasize the need for models to reflect the landfill dynamics associated with site  
433 specificity in each region to accurately assess gas collection system performance. Based on our  
434 measurement-based emission rates, the median collection effectiveness was 51%, aligning with studies by

435 Duan et al. (2022), who reported a range of 13% to 86% and a mean of 50% at Danish landfills using the  
436 same effectiveness definition (i.e., no oxidation accounted). In contrast, the ECCC FOD model estimates  
437 suggested an average collection effectiveness of only 20%, implying that collection systems were far less  
438 effective than they were in practice.

439 Extrapolating annual emissions from single-day measurements introduces uncertainty due to diurnal and  
440 seasonal variability in landfill emissions. However, models also require credible annual parameters that  
441 reflect landfill management and climate. Repeated measurements over multiple days, seasons, and years  
442 would improve accuracy and confidence. Our research contributes to a growing body of work informing  
443 inventory refinement and demonstrates the value of measurement-based approaches in optimizing model  
444 parameters and reducing uncertainty. Improving regulatory data collection from landfill operations and  
445 waste composition would further reduce uncertainty and support evidence-based policy development.

446 Canada's regulatory plan (Government of Canada, 2024) aims to reduce landfill methane emissions by  
447 50% below 2019 levels by 2030, through a new regulated framework based on surface methane  
448 concentration thresholds. Methane mitigation measures include the implementation or expansion of  
449 landfill methane control approaches such as landfill gas recovery systems, engineered biosystems, or  
450 methane flaring. Currently, about 150 large landfills in Canada have gas recovery systems, and expanding  
451 their installation at more sites could be a significant step. However, engineering calculations often assume  
452 75% and 90% collection efficiency for open and closed sites, respectively, which are much higher  
453 percentages than the one estimated from both measurement and FOD modeling. We hypothesize that  
454 active working face emissions, which can account for up to half the total landfill emissions and typically  
455 lack collection infrastructure (Scarpelli et al., 2024; Risk et al., 2025), might be overlooked. Without  
456 strategies that address active working faces and/or landfill methane reduction measures that account for  
457 lower collection efficiencies, Canada could fall short of its 50% reduction goal. Because of lower  
458 efficiency, collection systems might need to be deployed at a larger number of sites than planned.  
459 However, the goal could be achieved if the reduction strategies were complemented by policies

460 incentivizing active face collection. While only two landfills in Canada currently use active face  
461 collection systems, the technology is widely deployed in countries like the United Kingdom and could be  
462 scaled for use in Canada.

463 On a positive note, our measurements suggest that landfill methane emissions in the Canadian inventory  
464 tend to be overestimated. Emissions from arid regions were notably overpredicted. Our bias-corrected  
465 measurements, while offering a snapshot at a limited number of Canadian landfills, indicated that landfill  
466 methane inventories could be overstated by at least a factor of two, given the distribution of landfills  
467 across Canada.

468 The Canadian government has already demonstrated a commitment to inventory accuracy by  
469 implementing a measurement-informed methane inventory for the oil and gas sector—the first of its kind  
470 globally—by incorporating extensive aircraft site measurements annually to verify inventory estimates. A  
471 similar approach could be applied to the waste sector, where fewer sites and highly accurate methods,  
472 such as the ground-based tracer gas method, could make the initiative feasible and impactful.

## 473 Conclusion

474 This study provided a measurement-based assessment of methane emissions from Canadian landfills on a  
475 national scale, revealing systematic discrepancies between ECCC estimates based on the IPCC FOD  
476 model and the measurement-based estimates. Our findings showed that the ECCC modeling often  
477 overestimates emissions from cold and arid regions, while occasionally underestimating emissions from  
478 warmer, wetter climates. These mismatches highlight the need to refine inventory parameters, such as  
479 decay rates and oxidation assumptions, to better reflect Canada's climate diversity and site-specific  
480 landfill practices.

481 By integrating bias-corrected mobile survey measurements with regulatory data, we demonstrated that  
482 Canada's landfill methane inventory might be overstated—potentially by a factor of two. This suggests

483 that methane mitigation targets could be more achievable than anticipated, especially if active work faces  
484 and other high-emitting sources were effectively managed. However, improving inventory accuracy  
485 requires measurement campaigns, not necessarily similar to the survey approach used in this exploratory  
486 study, at a selection of sites that reflect all the landscape and climatic conditions encountered in Canada,  
487 and better regulatory data on landfill operations and waste composition to improve the input parameters  
488 of FOD models. Tracking emissions over an extended period at certain sites would provide valuable  
489 insights into how factors like weather or operational changes impact emission variability. As Canada  
490 moves towards ambitious waste sector methane reduction targets, aligning mitigation strategies with  
491 measurement-informed inventories will be critical to success. Our study underscores how valuable  
492 empirical data can be for validating models and supporting the case for scaling up measurement-informed  
493 approaches—already pioneered in Canada’s oil and gas sector—to achieve similar transparency and  
494 effectiveness in waste management.

495

496 References

- 497 Aronica, S, Bonanno, A, Piazza, V, Pignato, L, Trapani, S. 2009. Estimation of biogas produced by the  
498 landfill of Palermo, applying a Gaussian model. *Waste Management* 29(1): 233–239.  
499 <https://doi.org/10.1016/j.wasman.2008.02.026>
- 500 Ars, S, Vogel, F, Arrowsmith, C, Heerah, S, Knuckey, E, Lavoie, J, Lee, C, Pak, NM, Phillips, JL,  
501 Wunch, D. 2020. Investigation of the Spatial Distribution of Methane Sources in the Greater Toronto  
502 Area Using Mobile Gas Monitoring Systems. *Environmental Science and Technology* 54(24): 15671–  
503 15679. <https://doi.org/10.1021/acs.est.0c05386>
- 504 Börjesson, G, Svensson, BH. 1997. Seasonal and diurnal methane emissions from a landfill and their  
505 regulation by methane oxidation. *Waste Management and Research* 15(1): 33–54.  
506 <https://doi.org/10.1006/wmre.1996.0063>
- 507 Chanton, JP, Powelson, DK, Green, RB. 2009. Methane Oxidation in Landfill Cover Soils, is a 10%  
508 Default Value Reasonable? *Journal of Environmental Quality* 38(2): 654–663.  
509 <https://doi.org/10.2134/jeq2008.0221>
- 510 Chanton, J, Abichou, T, Langford, C, Spokas, K, Hater, G, Green, R, Goldsmith, D, Barlaz, MA. 2011.  
511 Observations on the methane oxidation capacity of landfill soils. *Waste Management* 31(5): 914–925.  
512 <https://doi.org/10.1016/j.wasman.2010.08.028>
- 513 Cusworth, DH, Duren, RM., Ayasse, AK, Jiorle, R, Howell, K, Aubrey, A, Green, RO, Eastwood, ML,  
514 Chapman, JW, Thorpe, AK, Heckler, J, Asner, GP, Smith, ML, Thoma, E, Krause, MJ, Heins, D,  
515 Thorneloe, S. 2024. Quantifying methane emissions from United States landfills. *Science* 383(6690):  
516 1499–1504. <https://doi.org/10.1126/science.adi7735>

517 Czepiel, P. M., Mosher, B., Crill, P. M., & Harriss, R. C. (1996a). Quantifying the effect of oxidation on  
518 landfill methane emissions. *Journal of Geophysical Research: Atmospheres*, *101*(D11), 16721–16729.  
519 <https://doi.org/10.1029/96JD00222>

520 Czepiel, P. M., Mosher, B., Harriss, R. C., Shorter, J. H., McManus, J. B., Kolb, C. E., Allwine, E., &  
521 Lamb, B. K. (1996b). Landfill methane emissions measured by enclosure and atmospheric tracer  
522 methods. *Journal of Geophysical Research: Atmospheres*, *101*(D11), 16711–16719.  
523 <https://doi.org/10.1029/96JD00864>

524 Duan, Z, Kjeldsen P, Scheutz, C. 2022. Efficiency of gas collection systems at Danish landfills and  
525 implications for regulations. *Waste Management* 139: 269–278.  
526 <https://doi.org/10.1016/j.wasman.2021.12.023>

527 Einola, J.-K. M., Kettunen, R. H., & Rintala, J. A. (2007). Responses of methane oxidation to temperature  
528 and water content in cover soil of a boreal landfill. *Soil Biology and Biochemistry*, *39*(5), 1156–1164.  
529 <https://doi.org/10.1016/j.soilbio.2006.12.022>

530 Environment and Climate Change Canada. 2022. Reducing methane emissions from Canada’s municipal  
531 solid waste landfills: Discussion paper. [https://www.canada.ca/en/environment-climate-  
532 change/services/canadian-environmental-protection-act-registry/reducing-methane-emissions-  
533 canada-municipal-solid-waste-landfills-discussion.html](https://www.canada.ca/en/environment-climate-change/services/canadian-environmental-protection-act-registry/reducing-methane-emissions-canada-municipal-solid-waste-landfills-discussion.html)

534 Environment and Climate Change Canada. 2025. National Inventory Report 1990–2023: Greenhouse Gas  
535 Sources and Sinks in Canada. Available online at: [canada.ca/ghg-inventory](https://www.canada.ca/ghg-inventory).

536 EPA (2023) Inventory of U.S. Greenhouse Gas Emissions and Sinks: 1990-2021. U.S. Environmental  
537 Protection Agency, EPA 430-R-23-002. [https://www.epa.gov/ghgemissions/inventory-us-greenhouse-  
538 gas-emissions-andsinks-1990-2021](https://www.epa.gov/ghgemissions/inventory-us-greenhouse-gas-emissions-andsinks-1990-2021).

539 Fallah-Shorshani, M, Shekarrizfard, M, Hatzopoulou, M. 2017. Integrating a street-canyon model with a  
540 regional Gaussian dispersion model for improved characterisation of near-road air pollution.  
541 *Atmospheric Environment* 153: 21–31. <https://doi.org/10.1016/j.atmosenv.2017.01.006>

542 Fjelsted, L., Christensen, A. G., Larsen, J. E., Kjeldsen, P., & Scheutz, C. (2019). Assessment of a landfill  
543 methane emission screening method using an unmanned aerial vehicle mounted thermal infrared  
544 camera – A field study. *Waste Management*, 87, 893–904.  
545 <https://doi.org/10.1016/j.wasman.2018.05.031>

546 Fougère, CR, Ghasemi, D, Khaleghi, A, Coyle, L, Bourlon, E, Li, H, Smith, M, Risk, D. 2025. Estimating  
547 Canadian landfill methane emissions from aircraft measurements [preprint]. *Social Science Research*  
548 *Network*. <https://doi.org/10.2139/ssrn.5186900>

549 Fredenslund, AM, Mønster, J, Kjeldsen, P, Scheutz, C. 2019. Development and implementation of a  
550 screening method to categorise the greenhouse gas mitigation potential of 91 landfills. *Waste*  
551 *Management* 87: 915–923. <https://doi.org/10.1016/j.wasman.2018.03.005>

552 Gillespie, LD, Ars, S, Alkadri, S, Urya, S, Khoo, T, Fraser, S, Vogel, F, Wunch, D. 2025. Estimating  
553 methane emissions from the waste sector in Southern Ontario using atmospheric measurements.  
554 *Journal of the Air and Waste Management Association* 75(2): 144–163.  
555 <https://doi.org/10.1080/10962247.2024.2435340>

556 Gollapalli, M, Kota, SH. 2018. Methane emissions from a landfill in north-east India: Performance of  
557 various landfill gas emission models. *Environmental Pollution* 234, 174–180.  
558 <https://doi.org/10.1016/j.envpol.2017.11.064>

559 Government of Canada. 2024. *Canada Gazette, Part 1, Volume 158, Number 26: Regulations Respecting*  
560 *the Reduction in the Release of Methane (Waste Sector)*. Government of Canada, Public Works and

561 Government Services Canada, Integrated Services Branch, Canada Gazette. [https://gazette.gc.ca/rp-](https://gazette.gc.ca/rp-pr/p1/2024/2024-06-29/html/reg5-eng.html)  
562 [pr/p1/2024/2024-06-29/html/reg5-eng.html](https://gazette.gc.ca/rp-pr/p1/2024/2024-06-29/html/reg5-eng.html)

563 Hossain, RI, Buntov, P, Dudak, Y, Martino, R, Fougere, C, Naseridoust, S, Bourlon, E, Lavoie, M,  
564 Khaleghi, A, Hall, C, Risk, D. 2025. A controlled release experiment for investigating methane  
565 measurement performance at landfills [preprint]. Earth ArXiv.  
566 <https://eartharxiv.org/repository/view/8985/>

567 (IPCC) Intergovernmental Panel on Climate Change. 2006. 2006 IPCC Guidelines for National  
568 Greenhouse Gas Inventories, Volume 4: Agriculture, Forestry and Other Land Use. IPCC National  
569 Greenhouse Gas Inventories Programme. Eggleston HS, Buendia L, Miwa K, Ngara T, Tanabe K  
570 (eds). Hayama

571 IPCC. 2000. Good Practice Guidance and Uncertainty Management in National Greenhouse Gas  
572 Inventories - J Penman, D Kruger, I Galbally, T Hiraishi, B Nyenzi, S Emmanul, L Buendia, R  
573 Hoppaus, T Martinsen, J Meijer, K Miwa and K Tanabe (Eds). ISBN 4-88788-000-6.  
574 [https://www.ipcc.ch/publication/good-practice-guidance-and-uncertainty-management-in-national-](https://www.ipcc.ch/publication/good-practice-guidance-and-uncertainty-management-in-national-greenhouse-gas-inventories/)  
575 [greenhouse-gas-inventories/](https://www.ipcc.ch/publication/good-practice-guidance-and-uncertainty-management-in-national-greenhouse-gas-inventories/)

576 Jain, P, Wally, J, Townsend, TG, Krause, M, Tolaymat, T. 2021. Greenhouse gas reporting data improves  
577 understanding of regional climate impact on landfill methane production and collection. *PLoS One*  
578 16(2): e0246334. <https://doi.org/10.1371/journal.pone.0246334>

579 Kissas, K., Ibrom, A., Kjeldsen, P., & Scheutz, C. (2022). Methane emission dynamics from a Danish  
580 landfill: The effect of changes in barometric pressure. *Waste Management*, 138, 234–242.  
581 <https://doi.org/10.1016/j.wasman.2021.11.043>

582 Krause, MJ, Chickering, GW, Townsend, GT, Reinhart, DR. 2016. Critical review of the methane  
583 generation potential of municipal solid waste. *Critical Reviews in Environmental Science and*  
584 *Technology* 46(13): 1117–1182. <https://doi.org/10.1080/10643389.2016.1204812>

585 J. Krause, M., Eades, W., Detwiler, N., Marro, D., Schwarber, A., & Tolaymat, T. (2023). Assessing  
586 moisture contributions from precipitation, waste, and leachate for active municipal solid waste  
587 landfills. *Journal of Environmental Management*, 344, 118443.  
588 <https://doi.org/10.1016/j.jenvman.2023.118443>

589 Lando, A. T., Nakayama, H., & Shimaoka, T. (2017). Application of portable gas detector in point and  
590 scanning method to estimate spatial distribution of methane emission in landfill. *Waste Management*,  
591 59, 255–266. <https://doi.org/10.1016/j.wasman.2016.10.033>

592 Liland, KH. 2015. 4S Peak Filling – baseline estimation by iterative mean suppression. *MethodsX* 2: 135–  
593 140. <https://doi.org/10.1016/j.mex.2015.02.009>

594 Matachiera, F, Manes, C, Beaven, RP, Rees-White, TC, Boano, F, Mønster, J, Scheutz, C. 2019.  
595 AERMOD as a Gaussian dispersion model for planning tracer gas dispersion tests for landfill methane  
596 emission quantification. *Waste Management* 87: 924–936.  
597 <https://doi.org/10.1016/j.wasman.2018.02.007>

598 Mohsen, RA, Abbassi, B. 2020. Prediction of greenhouse gas emissions from Ontario’s solid waste  
599 landfills using fuzzy logic based model. *Waste Management* 102: 743–750.  
600 <https://doi.org/10.1016/j.wasman.2019.11.035>

601 Omelchenko, M. V., Vasilyeva, L. V., & Zavarzin, G. A. (1993). Psychrophilic methanotroph from  
602 tundra soil. *Current Microbiology*, 27(5), 255–259. <https://doi.org/10.1007/BF01575988>

603 Park, JR., Moon, S, Ahn, YM, Kim, JY, Nam, K. 2005. Determination of Environmental Factors  
604 Influencing Methane Oxidation in a Sandy Landfill Cover Soil. *Environmental Technology* 26(1): 93–  
605 102. <https://doi.org/10.1080/09593332608618586>

606 Pipatti, R, Svardal, P. 2006. Solid waste disposal. In: Eggleston, S, Buendia, L, Miwa, K, Ngara, T.,  
607 Tanabe K, editors. 2006 IPCC Guidelines for National Greenhouse Gas Inventories. Vol 5.  
608 Intergovernmental Panel on Climate Change. [http://www.ipcc-](http://www.ipcc-nggip.iges.or.jp/public/2006gl/pdf/5_Volume5/V5_3_Ch3_SWDS.pdf)  
609 [nggip.iges.or.jp/public/2006gl/pdf/5\\_Volume5/V5\\_3\\_Ch3\\_SWDS.pdf](http://www.ipcc-nggip.iges.or.jp/public/2006gl/pdf/5_Volume5/V5_3_Ch3_SWDS.pdf)

610 Risk, D, Omid, A, Bourlon, E, Khaleghi, A, Perrine, G, Tarakki, N, Martino, R, Stuart, J. 2025. Active  
611 face emissions: An opportunity for reducing methane emissions in global waste management  
612 [preprint]. Earth ArXiv. <https://eartharxiv.org/repository/view/8891/>

613 Scarpelli, TR, Cusworth, DH, Duren, RM, Kim J, Heckler, J, Asner, GP, Thoma, E, Krause, MJ, Heins,  
614 D, Thorneloe, S. 2024. Investigating major sources of methane emissions at US landfills.  
615 *Environmental Science and Technology* 58(49): 21545–21556.  
616 <https://doi.org/10.1021/acs.est.4c07572>

617 Scheutz, C, Fredenslund, AM, Chanton, J, Pedersen, GB, Kjeldsen, P. 2011. Mitigation of methane  
618 emission from Fakse landfill using a biowindow system. *Waste Management* 31(5): 1018–1028.  
619 <https://doi.org/10.1016/j.wasman.2011.01.024>

620 Scheutz, C., & Kjeldsen, P. (2004). Environmental Factors Influencing Attenuation of Methane and  
621 Hydrochlorofluorocarbons in Landfill Cover Soils. *Journal of Environmental Quality*, 33(1), 72–79.  
622 <https://doi.org/10.2134/jeq2004.7200>

623 Spokas, KA, Bogner, JE. 2011. Limits and dynamics of methane oxidation in landfill cover soils. *Waste*  
624 *Management* 31(5): 823–832. <https://doi.org/10.1016/j.wasman.2009.12.018>

625 Thompson, S, Sawyer, J, Bonam, R, Valdivia, JE. 2009. Building a better methane generation model:  
626 Validating models with methane recovery rates from 35 Canadian landfills. *Waste Management* 29(7):  
627 2085–2091. <https://doi.org/10.1016/j.wasman.2009.02.004>

628 Turner, DB. 1964. A diffusion model for an urban area. *Journal of Applied Meteorology and Climatology*  
629 3(1): 83-91. [https://journals.ametsoc.org/view/journals/apme/3/1/1520-  
630 0450\\_1964\\_003\\_0083\\_admfau\\_2\\_0\\_co\\_2.xml](https://journals.ametsoc.org/view/journals/apme/3/1/1520-0450_1964_003_0083_admfau_2_0_co_2.xml)

631 Vu, HL, Ng, KTW, Richter, A. 2017. Optimization of first order decay gas generation model parameters  
632 for landfills located in cold semi-arid climates. *Waste Management* 69: 315–324.  
633 <https://doi.org/10.1016/j.wasman.2017.08.028>

634 Wang, Y, Fang, M, Lou, Z, He, H, Guo, Y, Pi, X, Wang, Y, Yin, K, Fei, X. 2024. Methane emissions  
635 from landfills differentially underestimated worldwide. *Nature Sustainability* 7(4): 496–507.  
636 <https://doi.org/10.1038/s41893-024-01307-9>

637 Xu, L., Lin, X., Amen, J., Welding, K., & McDermitt, D. (2014). Impact of changes in barometric  
638 pressure on landfill methane emission. *Global Biogeochemical Cycles*, 28(7), 679–695.  
639 <https://doi.org/10.1002/2013GB004571>

640

641

## 642 Contributions

643 Contributed to conception and design: DR, SF, FV

644 Contributed to acquisition of data: JS, RM, LC, DR

645 Contributed to analysis and interpretation of data: EB, DR, JS, RM, LC, EL, NB, SF, SA, FV

646 Drafted and/or revised the article: JS, DR, EB, RM, LC, EL, NB, SF, SA, FV

647 Approved the submitted version for publication: DR, EB, JS, RM, LC, EL, NB, SF, SA, FV

## 648 Acknowledgments

649 We thank all landfill operators who facilitated our work. We also appreciate the contributions of the  
650 skilled Environment and Climate Change Canada staff in the Pollutant Inventories and Reporting  
651 Division, Climate Research Division, and Waste Reduction and Management Division. We would like to  
652 thank Dr. Anders Fredenslund, of the Technical University of Denmark, as well as two anonymous  
653 reviewers for taking the time and effort necessary to review our manuscript. We sincerely appreciate their  
654 valuable comments and suggestions, which have helped us to improve the quality of the manuscript.

## 655 Funding information

656 Funding for the study was made available by Environment and Climate Change Canada through a  
657 Contribution Agreement to St. Francis Xavier University.

## 658 Competing interests

659 The authors declare that there are no competing financial or personal interests in relation to the work  
660 described.

## 661 Supplemental material

662 S1 Quantification of methane sources using mobile plume transects. This section describes the inversion  
663 approach based on the Gaussian Plume Model used to estimate methane emission rates from mobile  
664 measurements in this study.

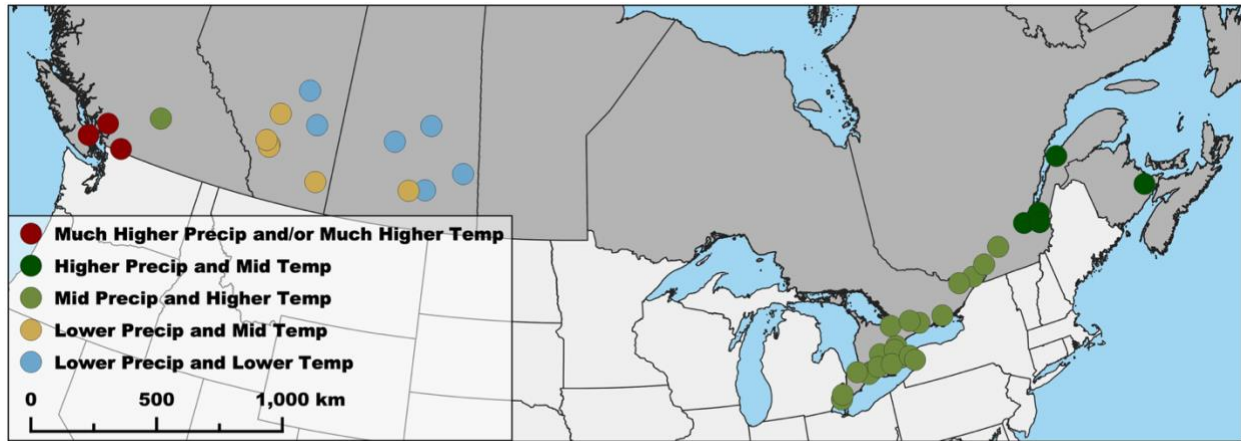
665 S2 Climate category definition. This section presents our exploration of climate parameters (precipitation,  
666 aridity, temperature, and climatic regions), which led to the definition of the selected climate categories.

667 These 2 sections are included in a PDF document, intitled  
668 “StFX\_FluxLab\_Canada\_Landfills\_Study\_Elementa\_Supplementary\_Material\_20260305.pdf”

669 Data accessibility statement

670 The data presented in this study are available at <https://doi.org/10.5683/SP3/PGJX03>. In this file, the  
671 landfill geolocation was removed to preserve site anonymity.

672



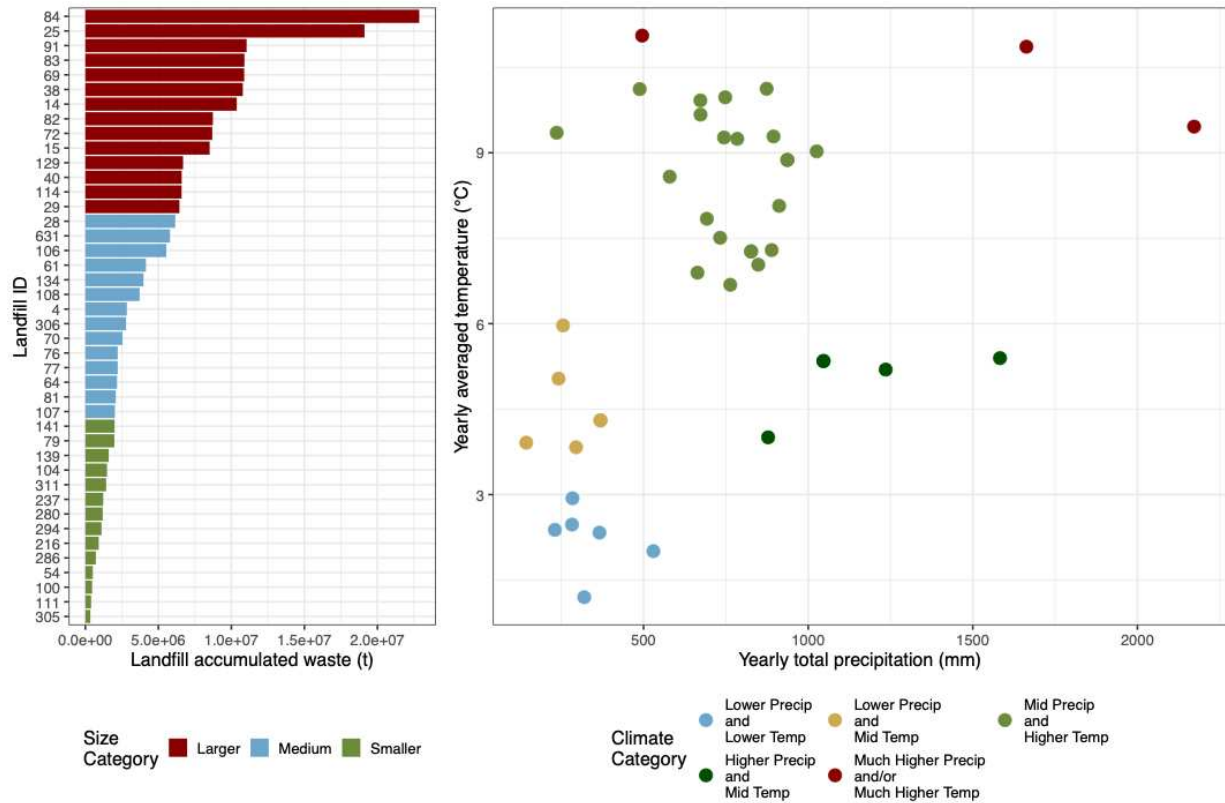
674

*CRS: Canada Albert Equal Area Conic. Provincial boundaries from Statistics Canada. State boundaries from US Census Bureau.*

675 **Figure 1. Locations of landfill sites.**

676 The colors represent the climate categories based on precipitation amounts and mean temperatures from

677 2018 to 2022.



678

679 **Figure 2. Landfill sizes and climate categories.**

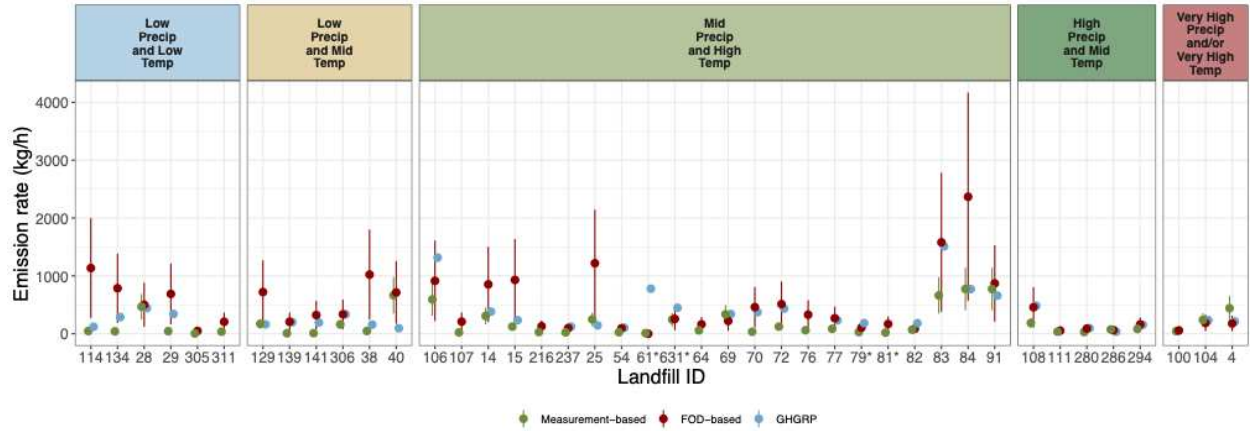
680 The left panel shows the distribution of landfill size, based on the accumulated waste tonnage as of 2022.

681 Sizes were divided into 3 groups, and the colors of the bars indicate the size category of each landfill. The

682 right panel represents the yearly average temperature (in °C) versus the yearly average precipitation

683 amount (in mm) for each landfill. Both quantities were calculated using weather data from ECCC stations

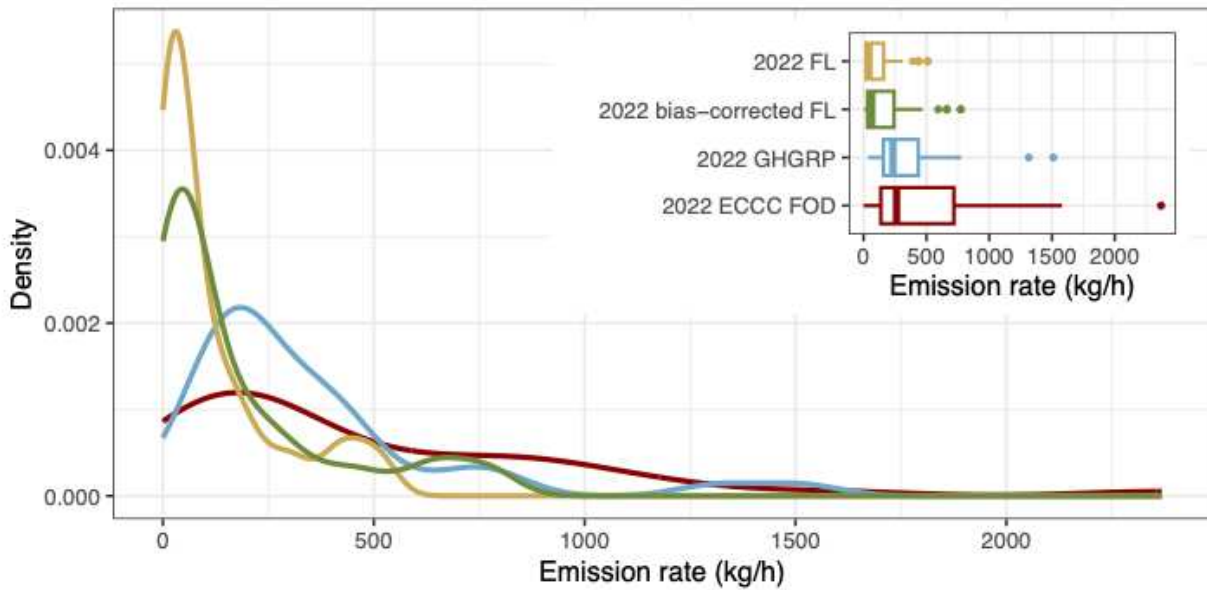
684 located within 50 km of each site. The colors indicate the climate clusters we used in this study.



685

686 **Figure 3. Bias-corrected measurement-based methane emission rate estimates, industry-reported**  
 687 **GHGRP estimates, and ECCC FOD model estimates.**

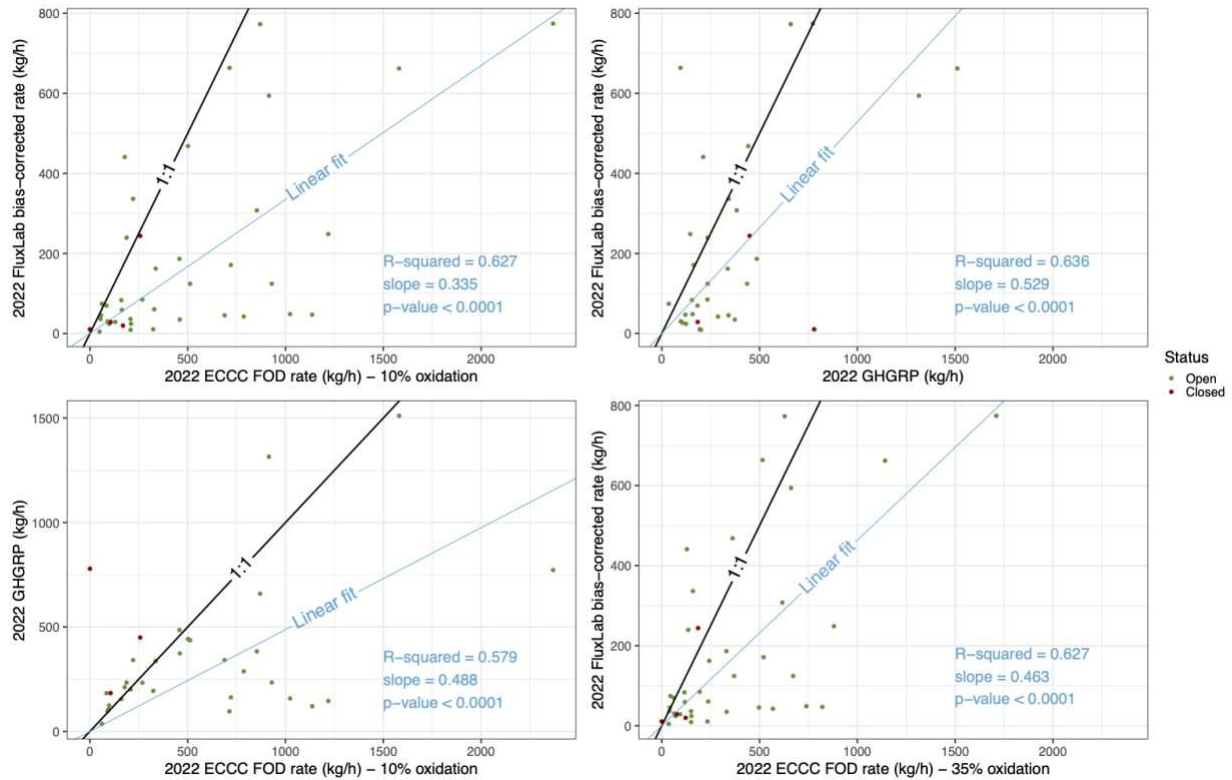
688 The figure shows the emission rate estimates used in this study. Bias-corrected, measurement-based  
 689 estimates are shown in green, ECCC FOD-based estimates in red, and GHGRP-reported estimates in blue.  
 690 Emissions are grouped by climate category to highlight where divergences occur. Closed landfills are  
 691 identified by an asterisk (\*) at the end of their identification number.



692

693 **Figure 4. Density plot of landfill direct and bias-corrected measurement-based emission rate**  
 694 **estimates, industry-reported GHGRP estimates, and ECCC FOD model estimates.**

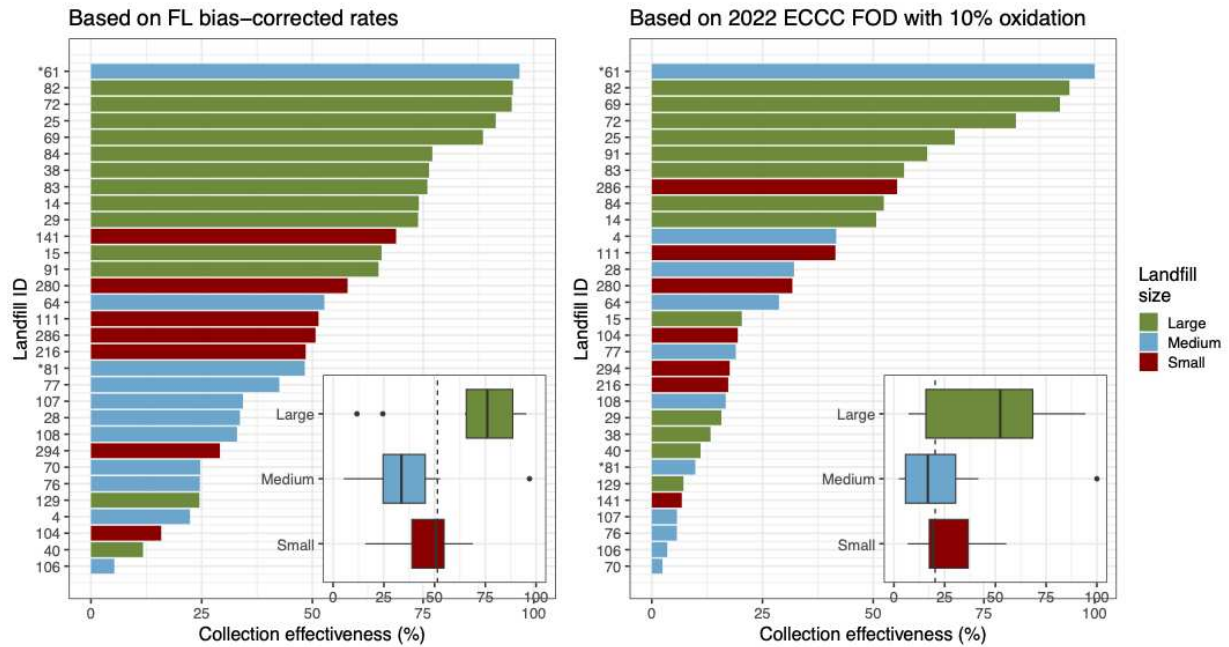
695 This figure highlights the difference in the distribution of each rate product. The inset illustrates how the  
 696 range of each rate product compares to the others.



697

698 **Figure 5. Linear regressions between the measurement-based rates, the ECCC modeled rates, and**  
 699 **the GHGRP reported rates.**

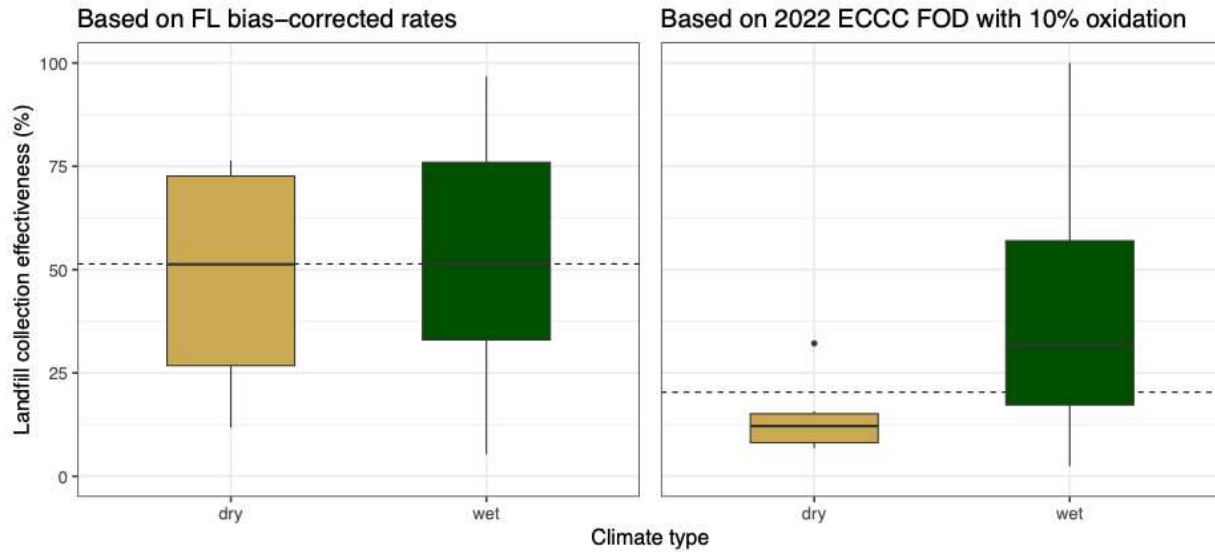
700 Left column: Measurement-based emission rate estimates (top) and GHGRP (bottom) versus ECCC FOD  
 701 model estimates. Right column: Measurement-based estimates versus GHGRP (top) and versus ECCC  
 702 FOD model with 35% methane oxidation (bottom). Note that the reported uncertainty for the IPCC FOD  
 703 modeled rate, using the standard parameters, is  $\pm 76\%$ , while the uncertainty for measurement-based  
 704 rates—estimated from the controlled release experiment—is 47.6%.



705

706 **Figure 6. Methane collection effectiveness.**

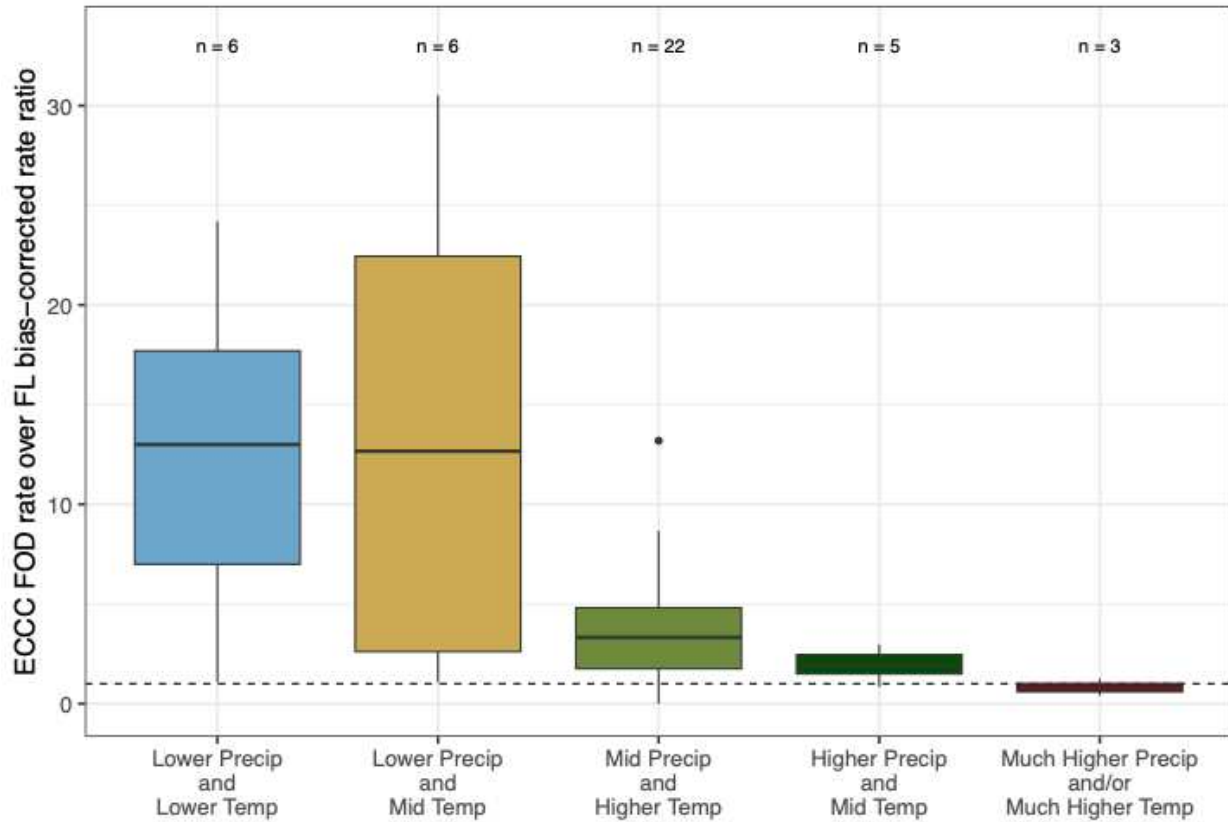
707 Collection effectiveness based on measurement-based rates (left) and ECCC FOD modeled rates with  
 708 10% oxidation (right), ordered by increasing collection efficiency. The insets show the effectiveness by  
 709 landfill size.



710

711 **Figure 7. Collection efficiency per type of climate, based on measurement-based rate (left) and on**  
 712 **ECCC FOD modeled rates (right).**

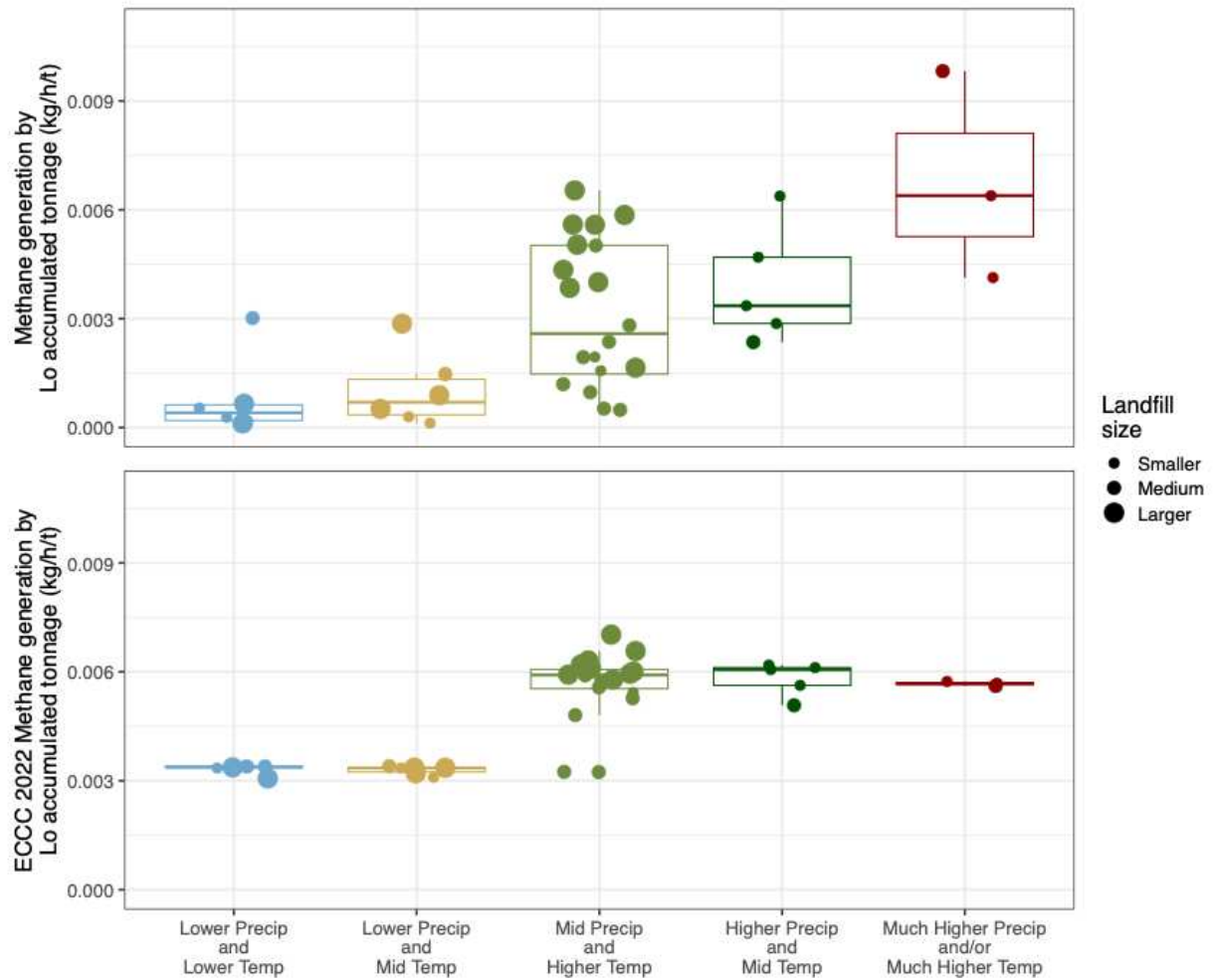
713 The “dry” type combines the two lower precipitation categories, and the “wet” one comprises the mid,  
 714 high, and higher precipitation climate categories. Efficiencies estimated using measurement-based rates  
 715 show no relationship with climate. In contrast, efficiencies from the FOD modeling reveal a sharp  
 716 difference between dry and wet climates.



717

718 **Figure 8. Ratio of measurement-based to ECCC FOD-modeled rate estimates across climate**  
 719 **categories.**

720 This figure highlights the amplitude of the difference between measurement-based rates and ECCC  
 721 modeled rates. The dashed line represents the 1:1 ratio. When boxes are above this line, ECCC rates are  
 722 higher than the measurement-based rates, and when ECCC rates are lower than the measurement-based  
 723 rates. The numbers on top of the boxes indicate the number of landfills in each climate category.



724

725 **Figure 9. Relation between methane generation per methane potential (L<sub>0</sub> accumulated tonnage)**  
 726 **and climate zone.**

727 In the top plot, the methane generation was calculated using 2022 reported collection volumes and 2022

728 measurement-based methane emissions. The 2022 methane generation rate from the ECCC FOD

729 modeling is used in the bottom plot.

730

731 Tables

732 **Table A. Bulk landfill waste decay rates (k in y<sup>-1</sup>) per climate categories based on our emission rate**  
733 **measurement and FOD modeling.**

734 Waste degradation depends on several factors, including moisture and temperature. Therefore, this table  
735 also presents the median annual precipitation and median annual temperature for each climate category.  
736 The median k values are reported with their second and third quartile ranges (Median [2<sup>nd</sup> quartile – 3<sup>rd</sup>  
737 quartile]).

---

<b>Climate category</b>	<b>Median precipitation (mm)</b>	<b>Median annual temperature (°C)</b>	<b>Measurement-based decay rate k (y<sup>-1</sup>)</b>	<b>FOD-based decay rate k (y<sup>-1</sup>)</b>
Lower Precip and Lower Temp	302	2.4	0.004 [0.002-0.006]	0.030 [0.030-0.030]
Lower Precip and Mid Temp	275	4.3	0.007 [0.003-0.014]	0.030 [0.028-0.030]
Mid Precip and Higher Temp	774	8.9	0.024 [0.013-0.046]	0.053 [0.049-0.055]
Higher Precip and Mid Temp	1046	5.3	0.032 [0.027-0.044]	0.055 [0.051-0.055]
Much Higher Precip and/or Much Higher Temp	1663	10.9	0.063 [0.052-0.081]	0.051 [0.051-0.051]

---

738

1  
2  
3  
4  
5  
6  
7  
8  
9  
10  
11  
12  
13

# Supplementary Material

for

## Canada's Landfill Methane Inventories: The Challenge of Accurate Modeled and Measurement-Based Emissions

Jordan Stuart<sup>1</sup>, David Risk<sup>1,\*</sup>, Evelise Bourlon<sup>1</sup>, Rebecca Martino<sup>1</sup>, Lindelwa Coyle<sup>1</sup>, Emil Laurin<sup>2</sup>,  
Nicholas Bishop<sup>2</sup>, Susan Fraser<sup>2</sup>, Sebastien Ars<sup>2</sup>, Felix Vogel<sup>2</sup>

<sup>1</sup>FluxLab, Department of Earth and Environmental Sciences, St. Francis Xavier University, Nova Scotia,  
Canada

<sup>2</sup>Environment and Climate Change Canada, Ontario, Canada

\*Corresponding author: David Risk [drisk@stfx.ca](mailto:drisk@stfx.ca)

Publication in Elementa—Science of the Anthropocene

October 3<sup>rd</sup>, 2025

14 Contents

15 S1 Quantification of methane sources using mobile plume transects .....4

16     Gaussian plume dispersion model and assumptions.....4

17     Gaussian Plume Inversion .....5

18     The damping effect of the gas sensor on the methane measurement.....6

19     Inversion approach.....6

20     Figures .....7

21     References.....9

22 S2 Climate category definition .....10

23 Figure S1. Two examples of field data comparison.....7

24 Figure S2. Comparison plots of our measured area versus each of the ECCC measured areas over multiple

25 transects. ....8

26 Figure S3. Illustration of the result from a laboratory measurement of our Picarro 2210i signal damping. .8

27 Figure S4. Map of the climatic regions of Canada .....11

28 Figure S5. Precipitation over temperature versus precipitation over potential evapotranspiration. This

29 figure shows how precipitation adds information to define climate categories. ....12

30 Figure S6. FAO aridity index versus yearly precipitation at the sites visited during our 2022 landfill

31 campaign. The color used in the top plot represents the ECCC FOD climate categories, and the color used

32 in the bottom plot are based on the climate categories used in this paper. ....13

33 Figure S7. Density kernel estimate plot of the aridity index distribution at our selection of sites. The

34 dashed vertical lines are located at the troughs between each mode/maximum.....14

35 Figure S8. Density kernel estimate plot of the aridity index distribution at our selection of sites. The

36 dashed vertical lines are located at the first trough and the change of slope on the second peak’s right

37 flank. ....14

38 Figure S9. Ratio of measurement-based to ECCC FOD-modeled rate estimates across climate categories.  
39 Similar to Figure 8 in the paper. .... 16  
40 Figure S10. Relation between methane generation per methane potential ( $L_0$  accumulated tonnage) and  
41 climate zone. Similar to Figure 9 in the paper. .... 17  
42  
43

## 44 S1 Quantification of methane sources using mobile plume transects

### 45 *Gaussian plume dispersion model and assumptions*

46 Numerous experimental field studies have been conducted to investigate the passive dispersion of non-  
47 reactive pollutants from continuous point sources, providing a foundation for the work of Sutton (1953)  
48 and Pasquill (1962). One important empirical feature is that the time-averaged concentration profiles are  
49 Gaussian in both the horizontal and vertical directions. The Pasquill-Gifford Gaussian plume model  
50 predicts concentrations from the distance to the source location, source height, source emission rate, wind  
51 speed, and dispersion coefficient. In this model, the pollutant is entirely reflected by the ground surface.  
52 Using a mathematical reference frame where the x axis is the downwind direction, the y axis the  
53 crosswind direction, and the z axis the vertical direction positive upward, the concentration  $\chi$  (in  $\mu\text{g}/\text{m}^3$ )  
54 in  $(x, y, z)$  for a continuous elevated point source located in  $(x_s, y_s, h)$  is:

$$\chi(x, y, z) = \frac{Q}{2\pi\sigma_y\sigma_z u} \times \exp\left(-\frac{(y - y_s)^2}{2\sigma_y^2}\right) \times \left\{ \exp\left[\frac{-(z - h)^2}{2\sigma_z^2}\right] + \exp\left[\frac{-(z + h)^2}{2\sigma_z^2}\right] \right\} \quad (1)$$

55 where  $\sigma_y$  and  $\sigma_z$  are the dispersion parameters (in m) in the crosswind and downwind direction, resp.,  $u$  is  
56 the wind speed (in m/s),  $h$  is the source height (in m), and  $Q$  is the emission rate (in  $\mu\text{g}/\text{s}$ ). The  
57 concentration  $\chi$  is implicitly a function of  $x$  through the dispersion parameters. These parameters describe  
58 the horizontal and vertical spread of the plume, and their equations (known as the  $\sigma$ -functions) were  
59 derived by Turner (1970) by fitting the Pasquill-Gifford curves (Gifford, 1961) for open country settings.  
60 The dispersion equations are keyed to the atmospheric stability classes that express the ratio of buoyancy  
61 over mechanical turbulence. Class A corresponds to the most unstable conditions, class D to neutral  
62 conditions, and class F to the most stable conditions. The turbulence intensity increases under unstable  
63 atmospheric conditions with the development of vertical air parcel updrafts, and it is reduced under stable  
64 atmospheric conditions that suppress those vertical updrafts. There are several atmospheric stability  
65 classification schemes, and they require a variable number of meteorological variables. The Pasquill  
66 classification (Pasquill, 1961) only requires the wind speed and an estimate of the solar radiation. In this

67 study, we utilized a classification by Tuner (1964), where the Pasquill scheme is refined by determining  
68 an index of solar radiation using the solar elevation angle (calculated using the location and the time) and  
69 the cloud cover and ceiling height, both standard weather measurements at most weather stations. The  
70 Gaussian plume model assumes continuous emission at a constant rate and constant meteorological  
71 conditions at least over the time of transport from the source to the sensor. The effect of plume rise at the  
72 source is not considered, but the effective height can replace the source height in the equation. The  
73 Gaussian plume model should not be applied under conditions of low wind speed ( $< 1\text{ m/s}$ ), and the  
74 equation presented here does not account for complex terrain, or deposition and chemical reaction within  
75 the plume during travel from the source to the sensor.

#### 76 *Gaussian Plume Inversion*

77 From Equation 1, the concentration from one source at one location  $(x, y, z)$  is linearly proportional to the  
78 source emission rate  $Q$ :

$$\chi(x, y, z) = Q \times \frac{\chi_{Q_1}(x, y, z)}{Q_1} = Q \times c(x, y, z) \quad (2)$$

79 where  $\chi_{Q_1}$  is the concentration for an emission rate of  $Q_1$  and  $c$  is the concentration from a source with a  
80 unitary emission rate (1 g/s). Each concentration measurement leads to one emission rate. A joint  
81 inversion of several concentration measurements can be performed to obtain a single emission rate. In  
82 matrix form, we have to solve:

$$\chi = \begin{bmatrix} \chi_1 \\ \chi_2 \\ \vdots \\ \chi_n \end{bmatrix} = Q \times \begin{bmatrix} c_1 \\ c_2 \\ \vdots \\ c_n \end{bmatrix} \quad (3)$$

83 where  $\chi$  is the vector of measured concentrations at locations 1 to  $n$ ,  $Q$  is the emission rate, and  $c$  is the  
84 vector of concentration for a 1g/s emission rate at the same  $n$  locations. This can be generalized for  
85 multiple emitting sources. The total measured concentration is the sum of each source contribution, and  
86 equation (3) can be rewritten as

$$\chi = \begin{bmatrix} \chi_1 \\ \chi_2 \\ \vdots \\ \chi_n \end{bmatrix} = Q_1 \times \begin{bmatrix} c_{11} \\ c_{12} \\ \vdots \\ c_{1n} \end{bmatrix} + Q_2 \times \begin{bmatrix} c_{21} \\ c_{22} \\ \vdots \\ c_{2n} \end{bmatrix} + \dots + Q_m \times \begin{bmatrix} c_{m1} \\ c_{m2} \\ \vdots \\ c_{mn} \end{bmatrix} \quad (4)$$

87 or

$$\chi = qC \quad (5)$$

88 where  $q$  is a vector of point emission rates from source 1 to  $m$  and  $C$  is an  $n \times m$  matrix of concentration  
 89 from source 1 to  $m$ , for a rate of  $1\text{g/s}$  and measurement locations 1 to  $n$ .

90

91 *The damping effect of the gas sensor on the methane measurement*

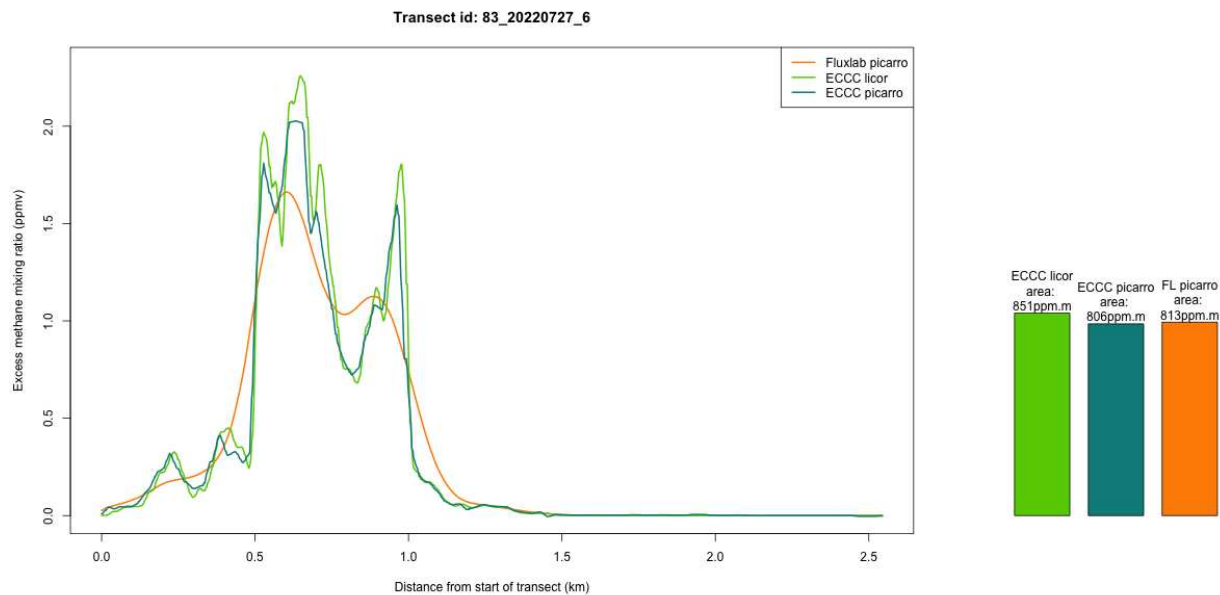
92 The response of cavity ring-down instruments, such as the ones we used in our mobile survey setting, to  
 93 an increase in methane varies with their flow rate and cavity size. We compared the height and area of the  
 94 methane enhancements recorded by several analyzers that were sampling simultaneously, both in the  
 95 laboratory (Figure S3) and in the field (Figure S1). We found that while slower instruments tend to damp  
 96 peaks relative to faster ones, the areas of the peaks were similar for all instruments (Figure S2). Therefore,  
 97 we used the integrated methane measurement as our data constraint in the inversion.

98 *Inversion approach*

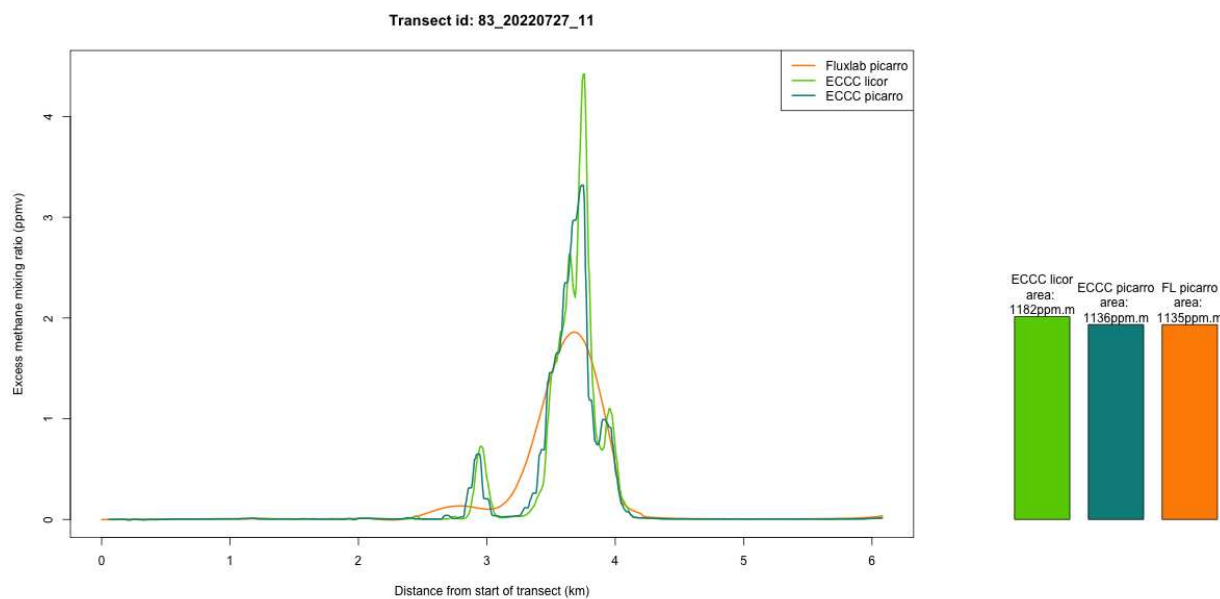
99 We want to minimize the difference between  $\chi$  and  $qC$ , with the constraint that all the elements of  $q$  are  
 100 positive, since our input locations are sources of methane, and not sinks. We solve this problem using  
 101 NonNegative Least Squares optimization:

102  $\min_q \| qC - \chi \|^2$  subject to  $q \geq 0$ .

103 We use the R interface to a Fortran 77 code by Lawson and Hanson (1995), based on the algorithm  
 104 described by Lawson and Hanson (1974).



106



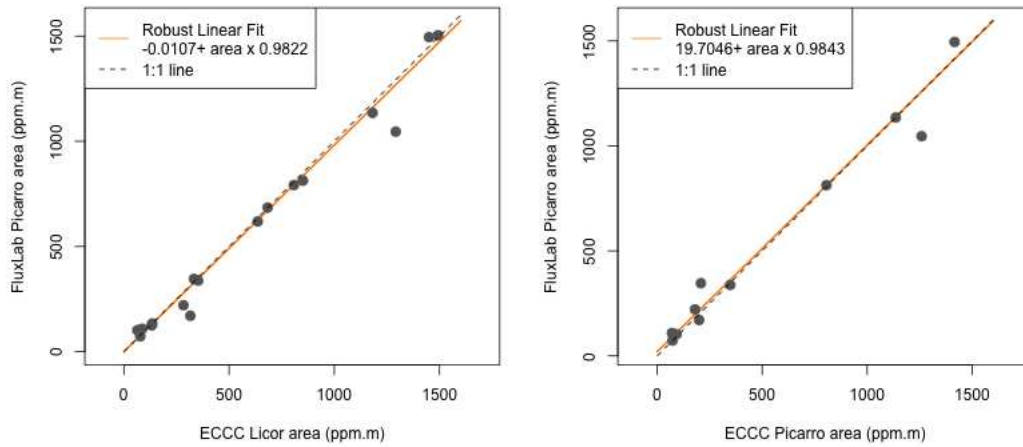
107

108 **Figure S1. Two examples of field data comparison.**

109 The plots on the left show the methane measurements, corrected for the ambient methane level, from  
 110 three instruments installed in two mobile laboratories conducting simultaneous surveys at the same  
 111 location. The ECCC mobile laboratory was equipped with a Licor LI810 and a Picarro G1301. Our setting

112 includes a Picarro 2210i, with a slower response than both ECCC instruments. The bars on the right show  
113 that, independent of the response of the instrument, the area under the curve is unchanged.

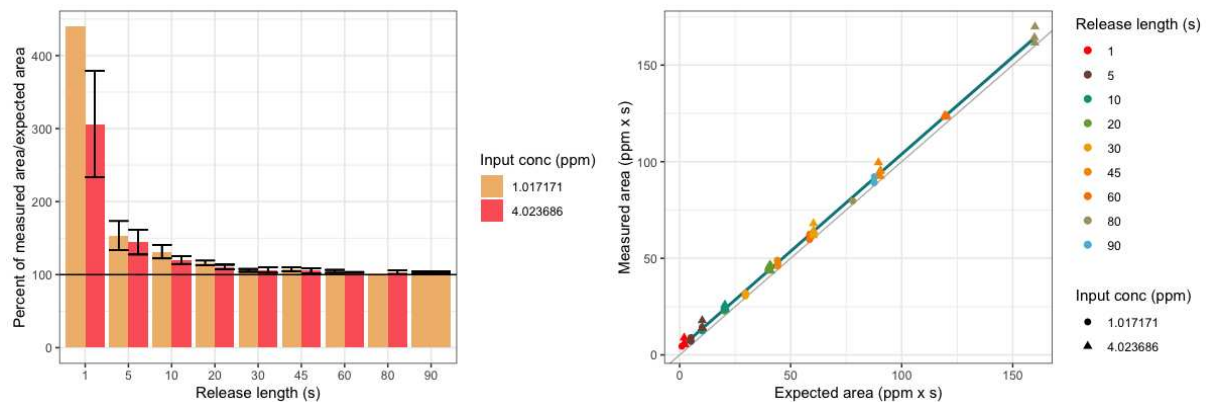
114



115

116 **Figure S2. Comparison plots of our measured area versus each of the ECCC measured areas over**  
117 **multiple transects.**

118 Left panel: ECCC Licor vs FluxLab Picarro concentration area. Right panel: ECCC Picarro vs FluxLab  
119 Picarro concentration area. Both fits are close to the 1:1 line.



120

121 **Figure S3. Illustration of the result from a laboratory measurement of our Picarro 2210i signal**  
122 **damping.**

123 Timing and length of release were measured, and we used 2 methane cylinders: one at 4ppmv (~2ppmv  
124 above ambient) and one at 1ppmv (~1ppmv below ambient). Left panel: Measured area as a percentage of  
125 the expected area versus the release duration. Right panel: Measured area versus expected area. The curve  
126 integration/area is overestimated by a factor of 3 to 4 for 1s-long releases, but the overestimation is below  
127 20% when the release is longer than 20s. The stretching of the anomaly seems to compensate for the  
128 damping of its amplitude.

129

### 130 *References*

131 Gifford, F. 1961. Use of Routine Meteorological Observations for Estimating Atmospheric Dispersion.  
132 Nuclear Safety, 2, 44-57.

133 Lawson CL, Hanson RJ. 1974. Solving Least Squares Problems. Prentice Hall, Englewood Cliffs, NJ.

134 Lawson CL, Hanson RJ. 1995. Solving Least Squares Problems. Classics in Applied Mathematics.  
135 SIAM, Philadelphia.

136 Pasquill, F. 1961. The Estimation of the Dispersion of Windborne Material. Meteorology Magazine, 90,  
137 33-40.

138 Pasquill, F. 1962. Atmospheric diffusion, Quarterly Journal of the Royal Meteorological Society,  
139 Vol.88(376), <https://doi.org/10.1002/qj.49708837622>

140 Sutton, OG. 1953. Micrometeorology, Quarterly Journal of the Royal Meteorological Society,  
141 Vol.79(341), <https://doi.org/10.1002/qj.49707934125>

142 Turner, DB. 1964. A Diffusion Model for an Urban Area, Journal of Applied Meteorology and  
143 Climatology, Vol.3(1), Pages 83-91, [https://doi.org/10.1175/1520-  
144 0450\(1964\)003%3C0083:ADMFAU%3E2.0.CO;2](https://doi.org/10.1175/1520-0450(1964)003%3C0083:ADMFAU%3E2.0.CO;2)

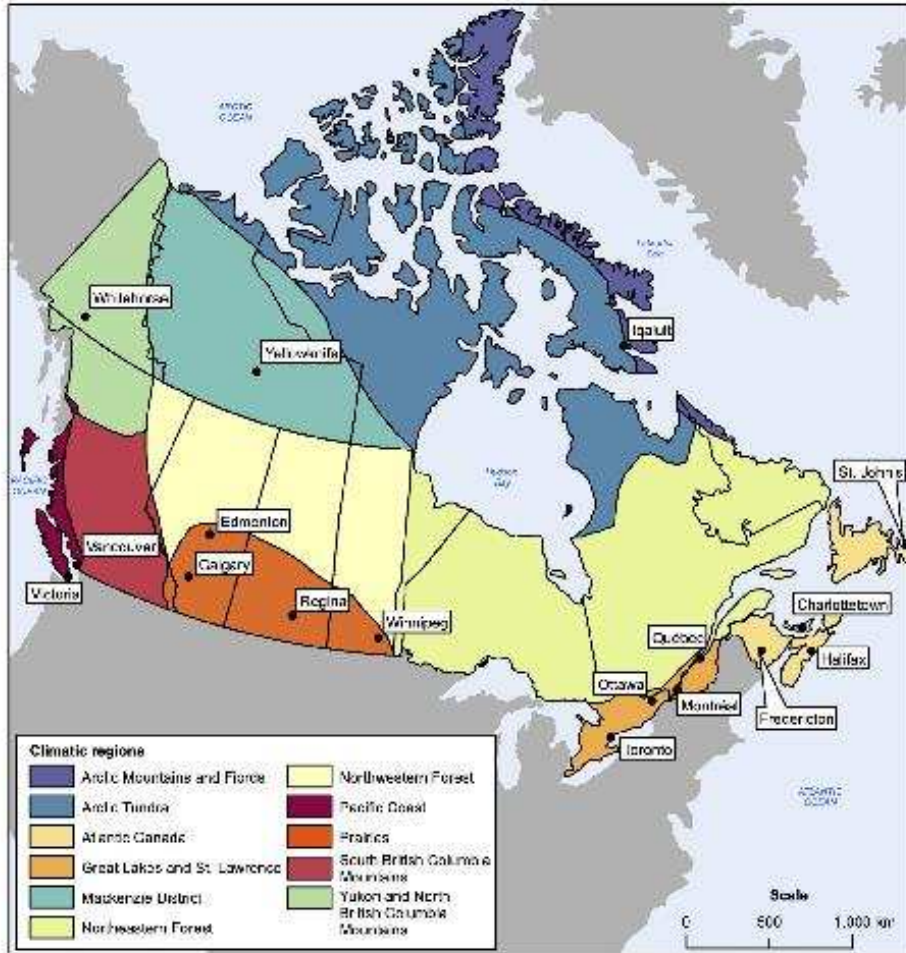
145 Turner, DB. 1970. Workbook of atmospheric dispersion estimates (Rev). U.S. Dept. of Health Education  
146 and Welfare, Public Health Service, Environmental Health Service, National Air Pollution Control  
147 Administration.

## 148 S2 Climate category definition

149 This section presents our exploration and definition of climate categories. As described in the main text,  
150 our initial approach used Köppen classes. One landfill falls under the BSk climate (Dry, Semi-arid  
151 steppe, Cold), three under the Cfb (Temperate, No dry season, Warm summer), one under the Dfc  
152 (Continental, No dry season, Cold summer), and the remaining 37 under the Dfb (Continental, No dry  
153 season, Warm summer).

154 Because three climate bins contained very few sampled sites, we instead used precipitation and  
155 temperature records from nearby ECCC airport ASOS weather stations, averaged over the five years  
156 preceding our campaign. Those are the climate categories presented in the paper.

157 To support our choice of climate categories, we include a map of Canada's climatic regions (Figure S4)  
158 produced by the Climate Research Branch of Environment Canada (the former name of ECCC). Our  
159 climate categories align well with those on this map, with the main difference being that the Gaspé  
160 Peninsula (on the south shore of the St. Lawrence River in Québec) is grouped with the Atlantic Canada  
161 region.

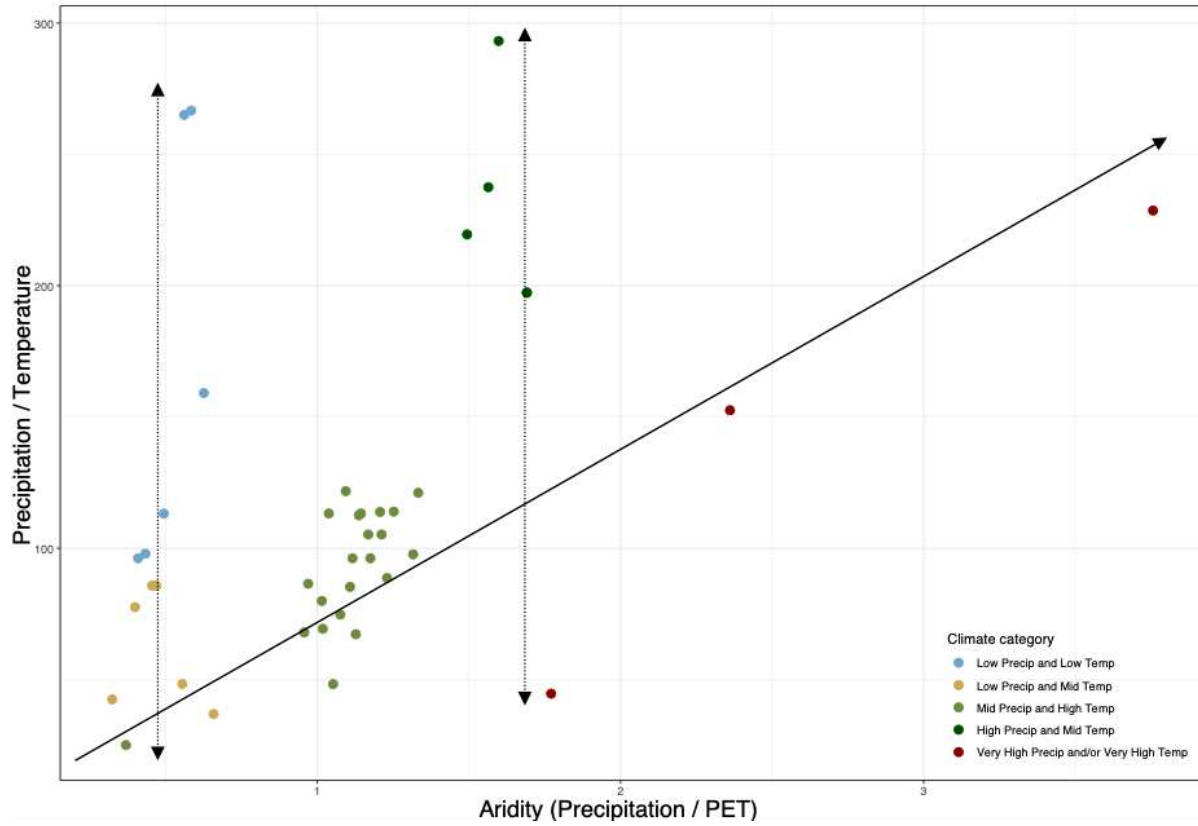


Source(s): Environment Canada, Atmospheric Environment Service, Climate Research Branch, 1998, Climate Trends and Variations Bulletin for Canada, Ottawa.

162

163 **Figure S4. Map of the climatic regions of Canada**

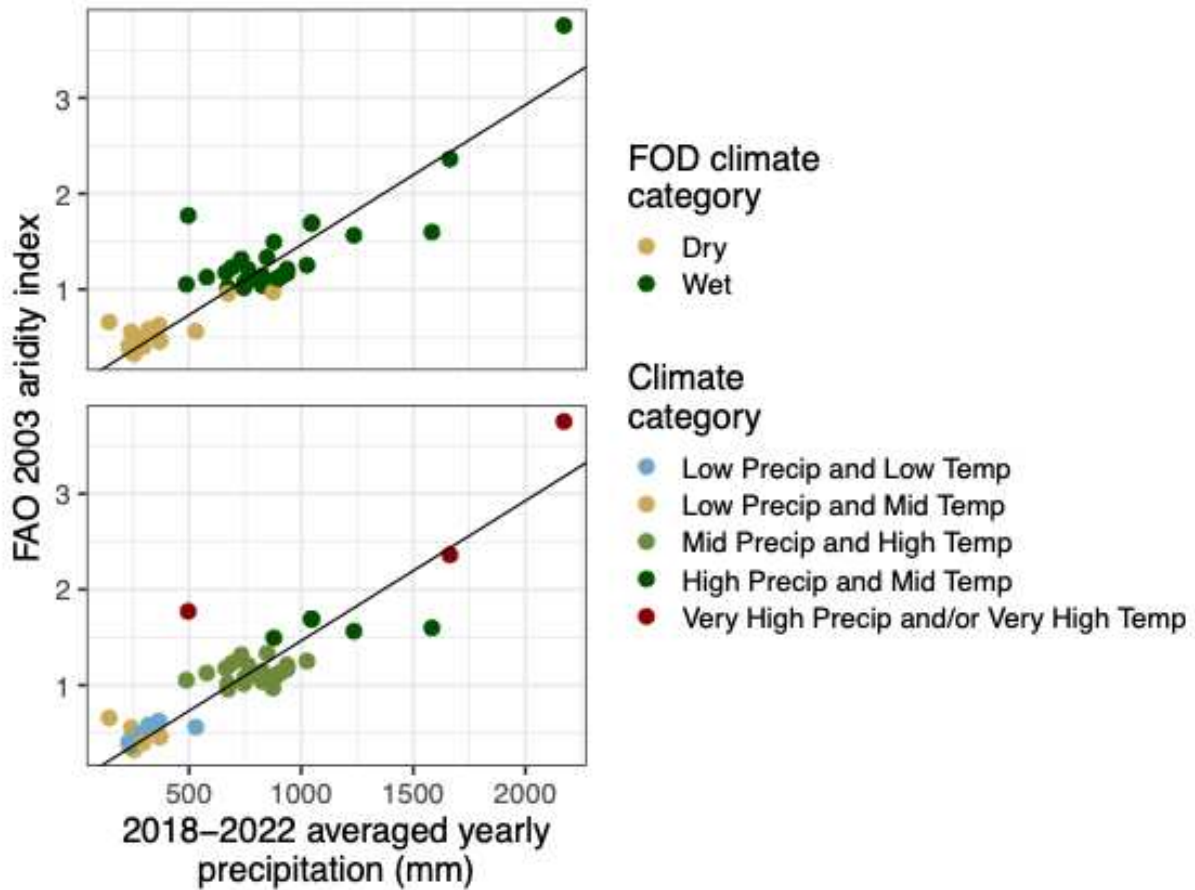
164 We also examined the ECCC climate classification based on the aridity index, defined as the ratio of  
 165 precipitation to potential evapotranspiration (PET). ECCC defines two climate zones across Canada: one  
 166 where PET exceeds precipitation (aridity < 1; “dry” climate) and another where PET is lower than  
 167 precipitation (aridity > 1; “wet” climate) (Figure S6). We obtained this index from the Food and  
 168 Agriculture Organization of the United Nations (FAO) data website  
 169 (<https://data.apps.fao.org/catalog/dataset/221072ae-2090-48a1-be6f-5a88f061431a>). At our selected sites,  
 170 the aridity and the precipitation are roughly linearly related (Figure S5); the PET do not vary much.  
 171 Adding the temperature to the precipitation or the aridity index adds another dimension to the climate  
 172 classification (Figure S5).



173

174  
175

Figure S5. Precipitation over temperature versus precipitation over potential evapotranspiration. This figure shows how precipitation adds information to define climate categories.



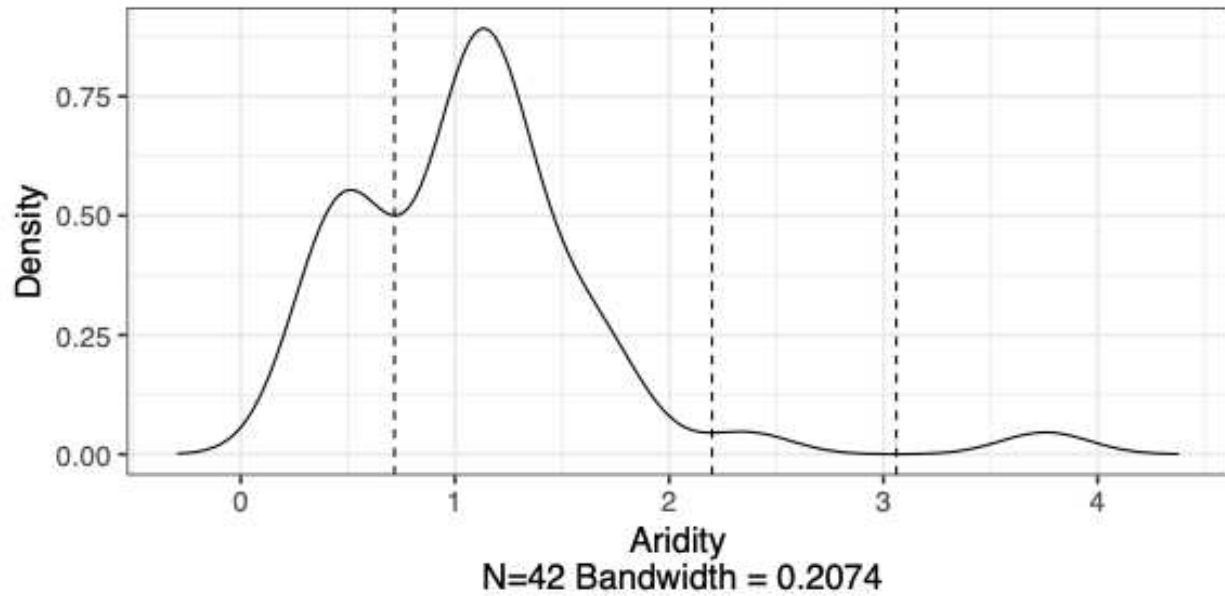
176

177 Figure S6. FAO aridity index versus yearly precipitation at the sites visited during our 2022 landfill campaign. The color  
 178 used in the top plot represents the ECCC FOD climate categories, and the color used in the bottom plot are based on the  
 179 climate categories used in this paper.

180 Our first attempt using the aridity index to define climate clusters consisted of using the aridity density

181 plot and using the troughs between the modes as cluster limits (located in aridity = 0.72, 2.20 and 3.06;

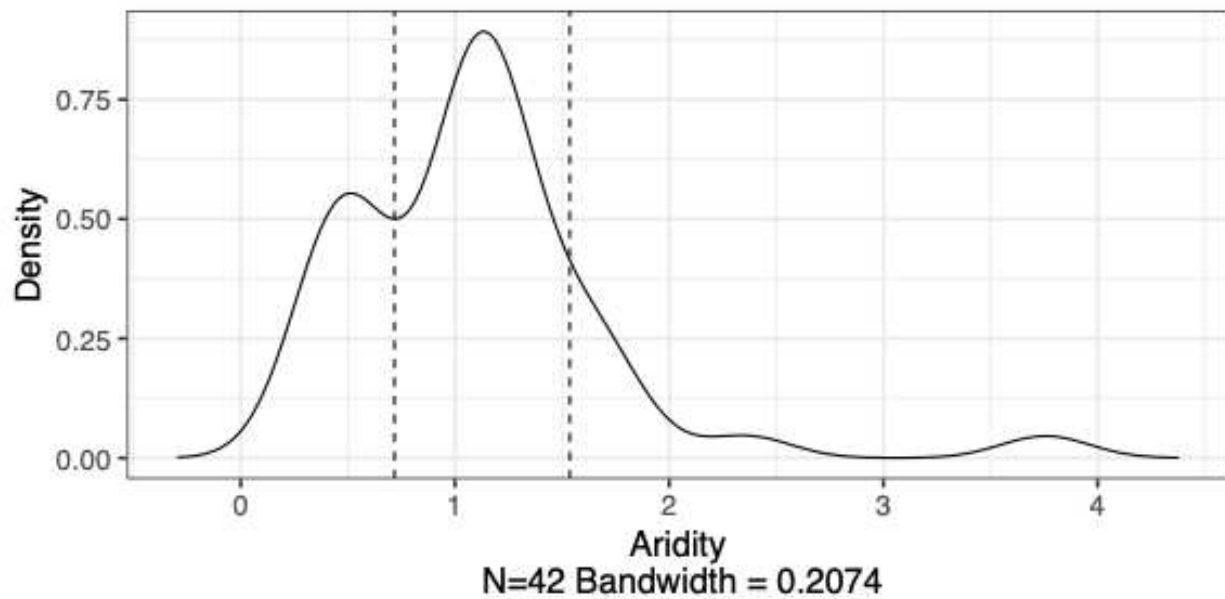
182 Figure S7). This resulted in 4 climate clusters, but two of them contained only one site.



183

184 Figure S7. Density kernel estimate plot of the aridity index distribution at our selection of sites. The dashed vertical lines  
 185 are located at the troughs between each mode/maximum.

186 We ended up defining 3 aridity-based clusters using the first trough and the slope change location of the  
 187 second peak's right flank (aridity index of ~1.54), as shown in Figure S8.



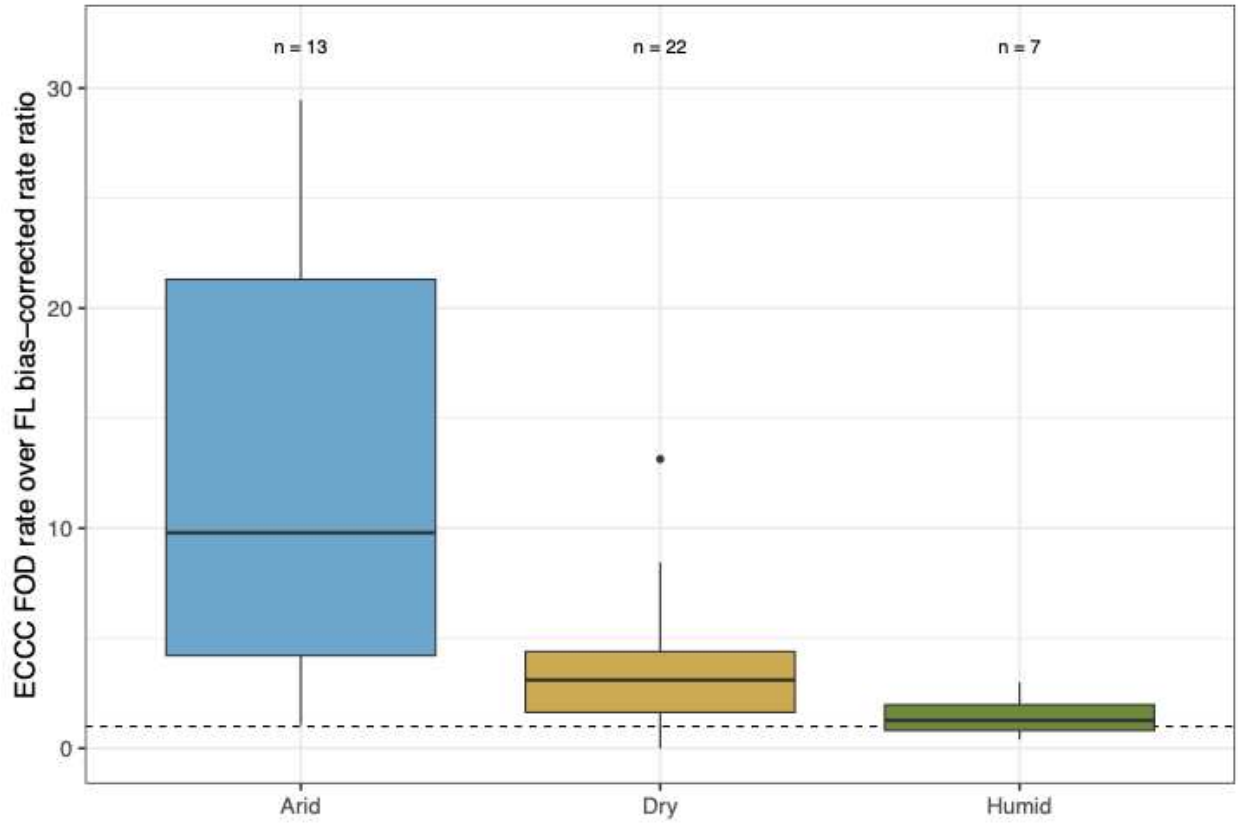
188

189 Figure S8. Density kernel estimate plot of the aridity index distribution at our selection of sites. The dashed vertical lines  
 190 are located at the first trough and the change of slope on the second peak's right flank.

191 The low aridity index “Arid” cluster combines our “lower precipitation and lower temperature” and  
192 “lower precipitation and mid temperature” classes (sites shown in yellow and blue in the paper figures),  
193 the mid aridity index “Dry” cluster corresponds to our “mid precipitation and higher temperature” class  
194 (in light green), and the high aridity index “Humid” cluster combines our “higher precipitation and mid  
195 temperature” and “much higher precipitation and/or much higher temperature” classes (in dark green and  
196 red). We reproduced two plots from the paper using this new classification. These two figures tell the  
197 same story as the original ones:

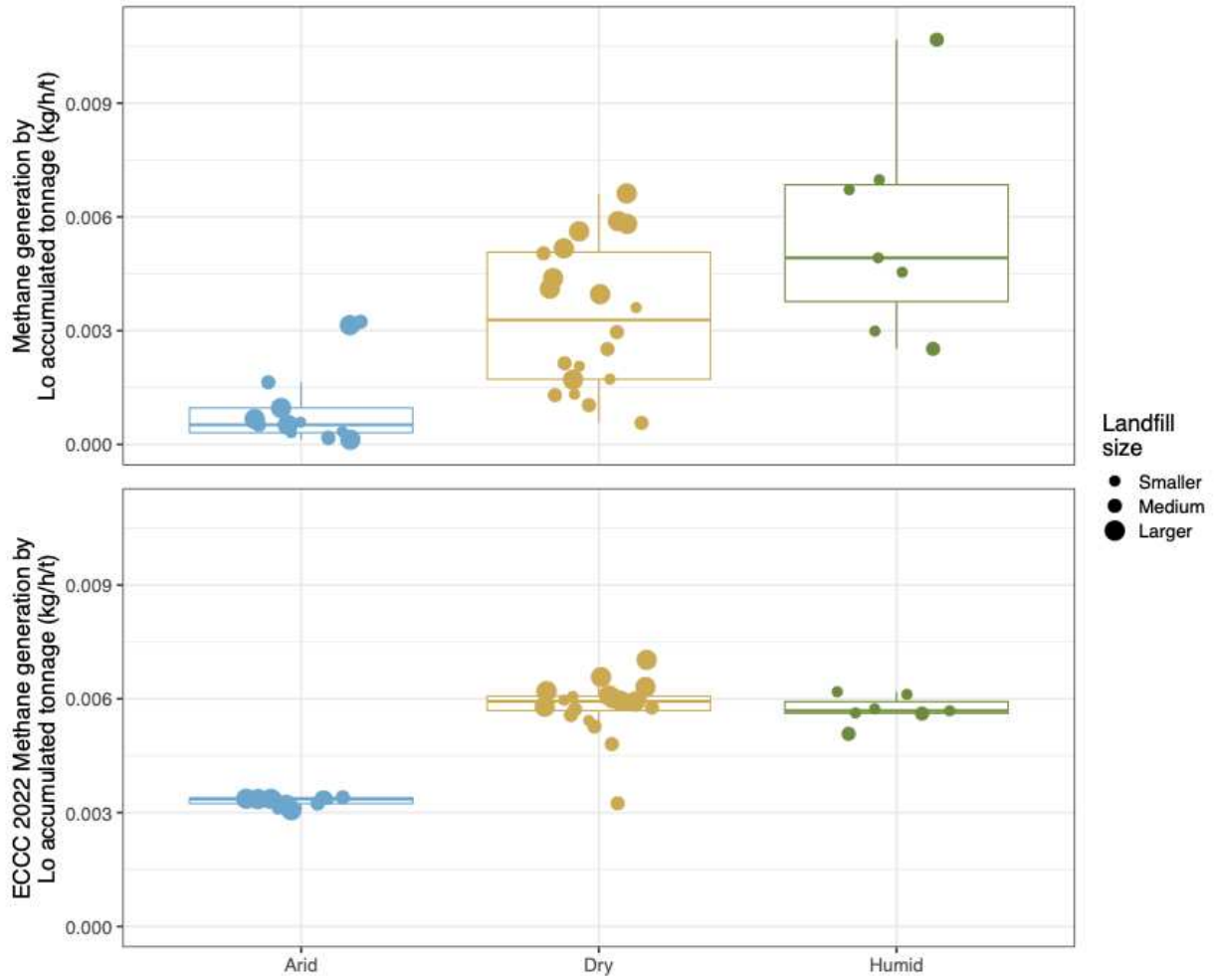
- 198 • Figure S9, comparable to Figure 8, shows that the discrepancy between measurement-based and  
199 FOD-model emission rate estimates is more pronounced in drier climates.
- 200 • Figure S10, comparable to Figure 9, displays the bimodal variability of the FOD methane  
201 generation-over- $L_0$  ratio, while the measurement-based ratio shows a more gradual increase.

202 Both aridity-based climate clusters and precipitation and the original temperature-based clusters lead to  
203 the same conclusions in this paper. The additional clusters in the chosen classification reinforce the visual  
204 perception of the variation of the measured emissions with climate regions. These clusters are not  
205 intended for modeling purposes. We suggest that the ECCC FOD modeling would benefit from adopting  
206 an alternative aridity-based climate clustering.



207

208 Figure S9. Ratio of measurement-based to ECCC FOD-modeled rate estimates across climate categories. Similar to Figure  
 209 8 in the paper.



210

211 Figure S10. Relation between methane generation per methane potential ( $L_0$  accumulated tonnage) and climate zone.  
 212 Similar to Figure 9 in the paper.

213